© 2016. Published by The Company of Biologists Ltd | Development (2016) 143, 609-622 doi:10.1242/dev.121731

RESEARCH ARTICLE

# Cannabinoid receptor signaling regulates liver development and metabolism

**Leah Y. Liu[1], Kristen Alexa[1], Mauricio Cortes[2], Stephanie Schatzman-Bone[1], Andrew J. Kim[1], Bani Mukhopadhyay[3], Resat Cinar[3], George Kunos[3], Trista E. North[2,4] and Wolfram Goessling[1,4,5,6,7,*]**

## ABSTRACT

Endocannabinoid (EC) signaling mediates psychotropic effects and regulates appetite. By contrast, potential roles in organ development and embryonic energy consumption remain unknown. Here, we demonstrate that genetic or chemical inhibition of cannabinoid receptor (Cnr) activity disrupts liver development and metabolic function in zebrafish (*Danio rerio*), impacting hepatic differentiation, but not endodermal specification: loss of *cannabinoid receptor 1* (*cnr1*) and *cnr2* activity leads to smaller livers with fewer hepatocytes, reduced liver-specific gene expression and proliferation. Functional assays reveal abnormal biliary anatomy and lipid handling. Adult *cnr2* mutants are susceptible to hepatic steatosis. Metabolomic analysis reveals reduced methionine content in Cnr mutants. Methionine supplementation rescues developmental and metabolic defects in Cnr mutant livers, suggesting a causal relationship between EC signaling, methionine deficiency and impaired liver development. The effect of Cnr on methionine metabolism is regulated by sterol regulatory element-binding transcription factors (Srebfs), as their overexpression rescues Cnr mutant liver phenotypes in a methionine-dependent manner. Our work describes a novel developmental role for EC signaling, whereby Cnr-mediated regulation of Srebfs and methionine metabolism impacts liver development and function.

**KEY WORDS: Cannabinoid receptor, Liver development, Methionine, Zebrafish, Mouse**

## INTRODUCTION

The energy requirements of developing embryos both influence and depend on the growth of essential metabolic organs. The factors impacting energy consumption and metabolism during embryogenesis, however, are not well understood. Each developmental stage may require the implementation of specific metabolic programs, and defects in metabolic processing or nutrient utilization could disrupt the differentiation and function of essential organs (Shyh-Chang et al., 2013). Alterations in developmental metabolism may also impact adult organ function through direct regulation of essential acetylation and methylation processes to alter the epigenetic control of development (Shyh-Chang et al., 2013; Sinclair and Watkins, 2014). Impairment of cellular proliferation pathways can disrupt organogenesis, thereby inhibiting normal physiological functions and leading to long-term consequences for adult metabolic homeostasis. Here, we show that endocannabinoid (EC) signaling is required for normal embryonic liver development and function. Disruptions of essential liver metabolic processes contribute to the development of diabetes, obesity and chronic liver disease. Elucidating the genetic pathways and mechanisms regulating developmental metabolism might inform early intervention strategies for individuals with genetic predisposition to metabolic disease.

The EC signaling pathway has predominantly been explored for its effects in the central nervous system (CNS), such as regulating appetite, mood and pain (Castillo et al., 2012). Primary ECs are bioactive fatty acid amides and esters synthesized in the CNS and the periphery, including 2-arachidonoyl glycerol (2-AG) (Sugiura et al., 1995) and arachidonoyl ethanolamide (anandamide, AEA) (Devane et al., 1992). Their effects are mediated by the G protein-coupled receptors Cnr1 and Cnr2. Cnr1 is primarily expressed in the CNS, where it promotes appetite control (Maccarrone et al., 2010), whereas Cnr2 acts in immune cells and the gastrointestinal tract (Munro et al., 1993). Although ECs regulate appetite in the CNS, how these ligands or their receptors influence embryonic metabolism and liver function via downstream targets is unknown.

Here, we discover that *cnr1* and *cnr2* are required for normal hepatocyte proliferation and differentiation during zebrafish development. Disrupted EC activity leads to decreased numbers of functionally immature hepatocytes, with impaired lipase activity and biliary lipid excretion. EC signaling orchestrates crucial metabolic functions during early nutritional transitions, and aberrations in liver histology and physiology in Cnr mutants persist in larval and adult zebrafish. Polar metabolomics analysis reveals dysregulation of methionine and its metabolic intermediates in Cnr mutants, a process mediated by sterol regulatory element-binding transcription factors (Srebfs). Supplementation with methionine and overexpression of *srebf1/2* both rescue the histological and metabolic defects in mutant larvae. Furthermore, long-term exposure of $cnr2^{-/-}$ mutants to methionine improves adult liver histology, with evidence for decreased hepatic fat accumulation. Our work uncovers a previously unrecognized relationship between embryonic EC signaling, liver development and metabolic homeostasis that impacts adult liver structure and function.

## RESULTS

### Inhibition of signaling through *cnr1* and *cnr2* impairs liver development

A chemical screen to identify novel regulators of liver development (Garnaas et al., 2012) revealed that the EC agonists anandamide, linoleoyl ethanolamide, mead acid ethanolamide, tetrahydrocannabinol (all Cnr1, Cnr2 agonists) and L759,633 (a

[1]Genetics Division, Brigham and Women's Hospital, Harvard Medical School, Boston, MA 02115, USA. [2]Department of Pathology, Beth Israel Deaconess Medical Center, Harvard Medical School, Boston, MA 02115, USA. [3]Laboratory of Physiological Studies, National Institute on Alcohol Abuse and Alcoholism, Bethesda, MD 20982, USA. [4]Harvard Stem Cell Institute, Cambridge, MA 02138, USA. [5]Gastroenterology Division, Brigham and Women's Hospital, Harvard Medical School, Boston, MA 02115, USA. [6]Dana-Farber Cancer Institute, Boston, MA 02215, USA. [7]Broad Institute of MIT and Harvard, Cambridge, MA 02142, USA.

*Author for correspondence (wgoessling@partners.org)

**Received 5 January 2015; Accepted 5 January 2016**

Development (2016) 143, 609-622 doi:10.1242/dev.121731

Cnr2 agonist) increased liver size, as determined by transgenic hepatocyte reporter *fatty acid binding protein 10a* (*fabp10a*):*GFP* expression at 72 h post fertilization (hpf). To confirm the screen results, embryos were exposed to Cnr modifiers (1-10 µM) from 18-72 hpf, and liver size was analyzed at 72 hpf by *in situ* hybridization (ISH) for *fabp10a*. Compared with DMSO-treated controls, the Cnr1/2 agonist O2545 (Martin, 2006), Cnr1 agonist leelamine hydrochloride (L-HCl), and the Cnr2 agonist JWH015 increased total *fabp10a* expression area, whereas the antagonists rimonabant (Cnr1) and AM630 (Cnr2) diminished liver size (Fig. 1A,B). Quantification of *fabp10a:GFP*-positive hepatocytes by fluorescence-activated cell sorting (FACS) confirmed the enhancing effect following agonist treatment (Fig. S1A). Together, these assays suggest an important role for EC signaling in liver development.

Expression of *cnr1* and *cnr2* is conserved in the zebrafish CNS at 24, 48 and 72 hpf (Fig. S1B) (Lam et al., 2006; Watson et al., 2008). Between 48 and 72 hpf, *cnr1* expression is also enriched in the liver, whereas *cnr2* is more broadly expressed, including the hepatic region, as determined by ISH (Fig. S1B). FACS-sorted *fabp10a:GFP* hepatocytes revealed strong *cnr1* expression by qRT-PCR (Fig. S1C). By contrast, *cnr2* expression was present in the hepatic region, but undetectable in the isolated hepatocyte fraction, a finding supported by previously established expression in whole liver, specifically the non-parenchymal liver cells, and its paracrine signaling functions in the liver (Julien et al., 2005; Teixeira-Clerc et al., 2010). Consistent with the chemical modulation studies, liver development was negatively impacted in both *cnr1* and *cnr2* morphants, each exhibiting smaller livers and hepatocyte numbers at 72 hpf (Fig. S2A,B).

To further validate the role of Cnr activity during hepatogenesis, $cnr1^{-/-}$ and $cnr2^{-/-}$ knockout zebrafish were generated using transcription activator-like effector nucleases (TALENs) (Sander et al., 2011) targeting the first exon of *cnr1* and *cnr2* (Fig. S2C,D): $cnr1^{-/-}$ and $cnr2^{-/-}$ mutants survived to adulthood, were fertile and exhibited no gross morphological defects or developmental delays (Fig. S2E). Compared with wild-type (WT) embryos and heterozygotes, *fabp10a* expression was significantly decreased in homozygous Cnr mutants at 72 hpf (Fig. 1C), as confirmed and quantified by liver morphometrics after ISH (Fig. 1D), FACS analysis of *fabp10a:GFP* embryos (Fig. 1E), and qRT-PCR for *fabp10a* (Fig. 1F). $cnr1^{-/-}$; $cnr2^{-/-}$ double mutants were also viable and exhibited liver phenotypes indistinguishable from single mutants by *fabp10a* expression and histology (Fig. 1G, Fig. S2F), suggesting a lack of compensation between the receptors, consistent with their different cellular expression. Together, these data confirm that both *cnr1* and *cnr2* are necessary for normal hepatogenesis.

Additional markers of differentiated hepatocytes, namely *group-specific component* (*vitamin D binding protein*) (*gc*), *secreted immunoglobulin domain 4* (*sid4*) and *transferrin-a* (*tfa*) at 72 hpf confirmed the validity of the findings (Fig. S3A-D). We examined endodermal and mesodermal organs to assess liver specificity: in $cnr1^{-/-}$ and $cnr2^{-/-}$ mutants, intestinal development was disrupted, with decreased *fabp2* expression at 72 hpf (Fig. S4A); by contrast, exocrine pancreas development (*trypsin* at 72 hpf) was unaffected, as were kidney (*pax2a*) and heart (*cmlc2*; also known as *myl7*) (not shown). Importantly, expression of the endodermal marker *foxa3* and the hepatic progenitor markers *hhex* and *prox1* was unchanged in Cnr homozygous mutants, heterozygotes, or morphants at 48 and 72 hpf (Fig. 2A,B, Fig. S3E-G and Fig. S4B). EC signaling therefore impacts differentiation and/or proliferation of committed hepatocytes or hepatic progenitors, whereas hepatoblasts are properly specified from early endoderm.

To further delineate the temporal importance of EC signaling and the target cell population during endoderm formation and hepatic differentiation, embryos were exposed to Cnr agonists from 24-48 hpf (hepatoblast formation) or 48-72 hpf (hepatocyte differentiation and proliferation). Only exposure from 48-72 hpf impacted liver size (Fig. 2C,D) at 72 hpf, supporting a role in hepatocyte differentiation and/or expansion, consistent with our observation of the timing of hepatic *cnr1* and *cnr2* expression.

### $cnr1^{-/-}$ and $cnr2^{-/-}$ mutants exhibit disrupted hepatocyte proliferation

We examined later time points to determine if alterations in hepatocyte differentiation persisted beyond initial liver growth stages: defects in total liver cell number and liver expression area were still observed at 96 hpf in $cnr1^{-/-}$ and $cnr2^{-/-}$ mutants, but were less pronounced by 120 hpf (Fig. S4C-E). Mutants did not exhibit increased TUNEL staining at 96 hpf, excluding cell death as a contributor (Fig. S4F). EdU incorporation assays at 72, 96 and 120 hpf in *fabp10a:GFP* embryos (Fig. 2E,F) revealed reduced proliferation at 72 hpf in $cnr1^{-/-}$; *fabp10a:GFP* and $cnr2^{-/-}$; *fabp10a:GFP* embryos, indicating that loss of EC signaling results in hepatocyte proliferation defects. However, by 96 hpf, there is no detectable difference in EdU incorporation rate, although the liver remains smaller in the mutant until normalization of liver size at 120 hpf. Given the gradual normalization of liver size in Cnr mutants by 120 hpf in the absence of hyperproliferation, presumably delayed or suboptimal differentiation and subsequent cellular remodeling of existing hepatic progenitors must occur.

To assess additional morphological defects, hepatic cellular morphology was examined by histology at 120 hpf. $cnr1^{-/-}$ and $cnr2^{-/-}$ hepatocytes have increased cytoplasmic staining and a decreased nucleus-to-cytoplasm ratio compared with WT, whereas overall hepatocyte size remains unchanged (Fig. 3A). These data indicate that, despite apparent recovery of the domain of *fabp10a* expression at 120 hpf, histological features remain abnormal in Cnr mutant larvae, consistent with a persistent impact on hepatocyte differentiation.

To confirm whether EC signaling affects the maturation of other hepatic cell types, we examined the biliary network using the Notch reporter *tp1bglob:eGFP* (Parsons et al., 2009). Morpholino-mediated knockdown of *cnr1* or *cnr2* decreased biliary development, including branching, as visualized by confocal microscopy at 96 hpf (Fig. 3B). The biliary marker 2F11 revealed compact and evenly distributed biliary epithelial cells in larval sections at 120 hpf; by contrast, $cnr1^{-/-}$ and $cnr2^{-/-}$ mutants showed impaired biliary tree formation, with a clustered and less uniform appearance (Fig. 3C).

To confirm these abnormalities and visualize hepatic lipid metabolism *in vivo*, BODIPY C5 fluorophore was administered, which labels all organs in which metabolites accumulate (Carten et al., 2011): control livers exhibit highly branched bile ducts at 6 days post fertilization (dpf); by contrast, both $cnr1^{-/-}$ and $cnr2^{-/-}$ mutants demonstrate decreased branching. In addition, $cnr2^{-/-}$ livers accumulate lipid droplets, indicative of abnormal lipid handling (Fig. 3D). To further characterize the role of Cnr in hepatic lipid metabolism, embryos were exposed to the lipase reporter PED6, leading to a fluorescent signal in intestine and gallbladder upon lipase-mediated cleavage (Farber, 2001). $cnr1^{-/-}$ and $cnr2^{-/-}$ mutants demonstrate little or undetectable gallbladder fluorescence at 120 hpf, indicative of reduced lipase activity

Development (2016) 143, 609-622 doi:10.1242/dev.121731

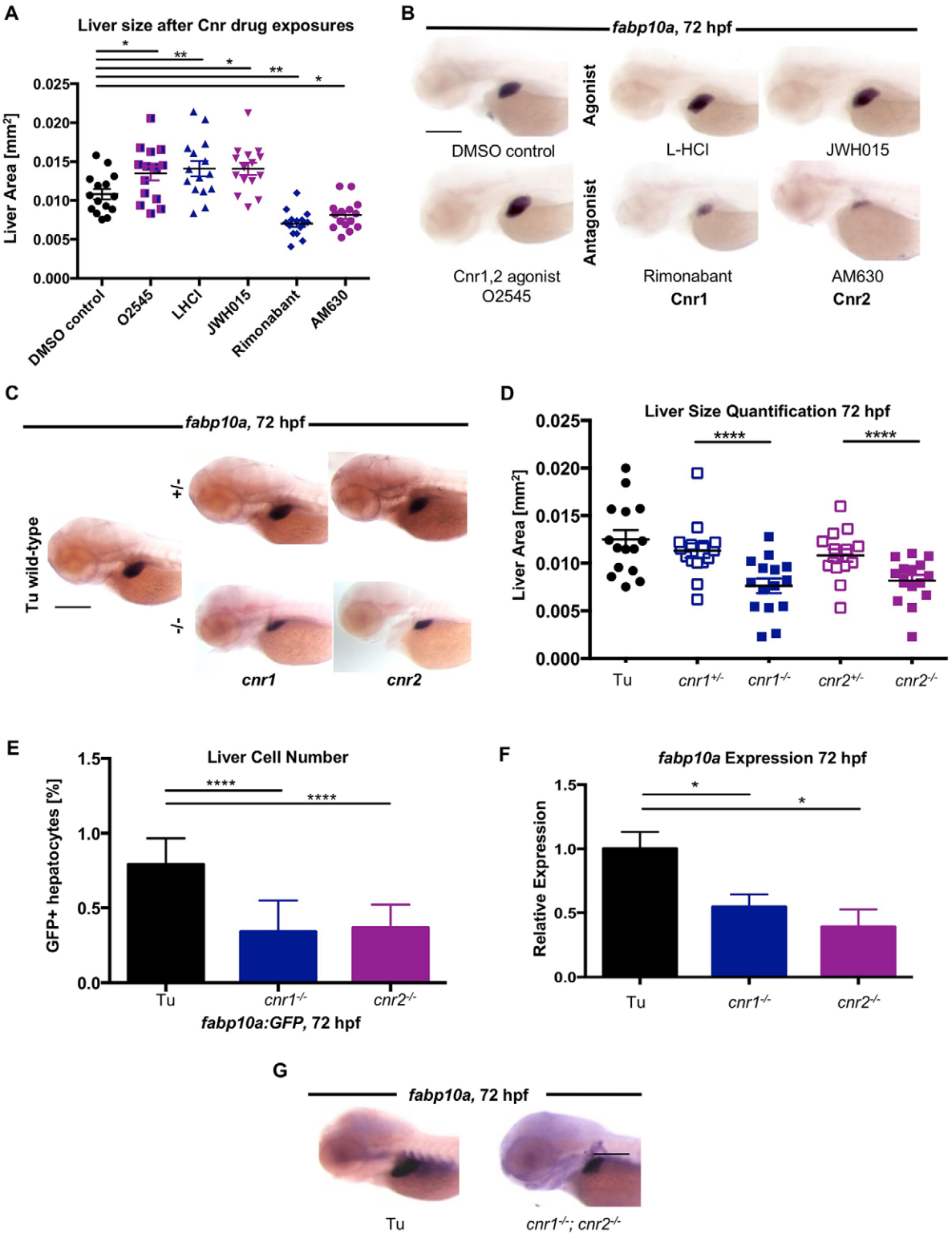


**Fig. 1. Chemical and genetic modulation of endocannabinoid (EC) signaling alters liver size and cell number during zebrafish development.** (A) Quantification of liver size in DMSO-treated and Cnr agonist/antagonist-treated WT embryos from 18-72 hpf. Agonists (O2545, L-HCl, JWH015) increased, whereas antagonists (rimonabant, AM630) decreased, liver size. ***P*<0.01, DMSO versus L-HCl or rimonabant; **P*<0.05, DMSO versus O2545, JWH015 or AM630. (B) Representative ISH images for *fabp10a* in zebrafish embryos after treatment with cannabinoid drugs from 18-72 hpf. (C) Representative ISH images showing decreased *fabp10a* expression in $cnr1^{-/-}$ and $cnr2^{-/-}$ mutants compared with WT and heterozygous siblings. (D) Quantification of liver size by measurement of *fabp10a* expression area after ISH in WT (Tu), heterozygous, and homozygous $cnr1^{-/-}$ and $cnr2^{-/-}$ mutants at 72 hpf. Results represent one independent experiment of triplicate experiments yielding similar results. *****P*<0.0001, for $cnr1^{+/-}$ versus $cnr1^{-/-}$ and for $cnr2^{+/-}$ versus $cnr2^{-/-}$. (E) FACS quantification of *fabp10a:GFP* hepatocyte number in WT compared with $cnr1^{-/-}$ and $cnr2^{-/-}$ mutants at 72 hpf. The fraction of $GFP^{+}$ cells was normalized to controls. *n*=3 pooled samples of ten embryos. *****P*<0.0001, *fabp10a:GFP* versus $cnr1^{-/-}$ and $cnr2^{-/-}$. (F) Quantification of *fabp10a* expression in WT and Cnr mutants by qRT-PCR at 72 hpf. *n*=3 pooled samples of 20 embryos. **P*<0.05. (G) ISH for *fabp10a* in $cnr1^{-/-}; cnr2^{-/-}$ double mutants at 72 hpf. All error bars show mean±s.e.m. *P*-values by one-way ANOVA. Scale bars: 0.2 mm.

Development (2016) 143, 609-622 doi:10.1242/dev.121731

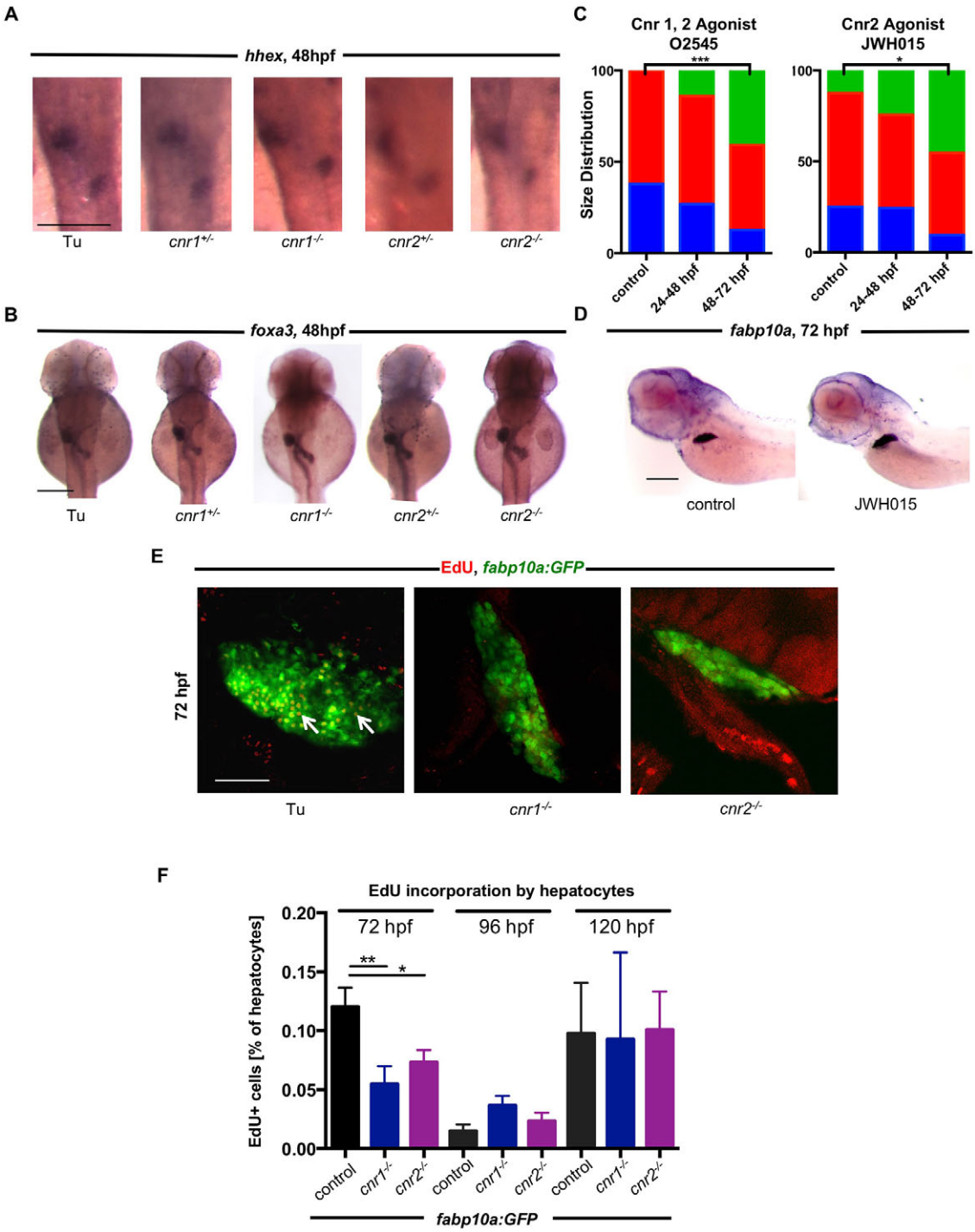


**Fig. 2. Hepatocyte proliferation is disrupted in Cnr mutants without impairment of hepatic progenitors.** (A) ISH for *hhex* at 48 hpf in WT (16 abnormal/89 observed), *cnr1*$^{+/-}$ (6/28 abnormal), *cnr2*$^{+/-}$ (5/32 abnormal), *cnr1*$^{-/-}$ (19/70 abnormal) and *cnr2*$^{-/-}$ (7/35 abnormal) embryos, revealing no significant differences in the hepatic progenitor population. (B) *foxa3* ISH at 48 hpf in WT (19/96 abnormal), *cnr1*$^{+/-}$ (4/29 abnormal), *cnr2*$^{+/-}$ (5/30 abnormal), *cnr1*$^{-/-}$ (12/54 abnormal) and *cnr2*$^{-/-}$ (4/40 abnormal) embryos, showing no differences in the endoderm population. (C) Relative frequency of liver size distribution of zebrafish embryos treated with Cnr agonists during different stages of liver development, as assessed by *fabp10a* expression at 72 hpf. Treatment with the Cnr1/2 agonist O2545 (1 µM) or the Cnr2 agonist JWH015 (1 µM) only from 48-72 hpf increased liver size, whereas earlier treatment had no effect. Normal liver size, red; small liver, blue; large liver, green. *n*>30 embryos. Chi-squared analysis. O2545, ***$P$<0.001 control versus 48-72 hpf treatment; JWH015, *$P$<0.05 control versus 48-72 hpf treatment. (D) Treatment with JWH015 from 48-72 hpf increases *fabp10a* expression in zebrafish embryos at 72 hpf. (E) Confocal projections of *fabp10a:GFP* livers at 72 hpf after EdU incorporation. EdU-positive hepatocytes are represented by colocalization (arrows) of red EdU staining and hepatocyte-specific GFP expression. (F) FACS quantification of EdU-positive cells as a percentage of the GFP$^{+}$ population at 72, 96 and 120 hpf. At 72 hpf there is less EdU incorporation compared with controls, indicating a decreased proliferation rate. At 96 and 120 hpf, there is no difference in the proliferation rate. Mean±s.e.m., *n*=3-8 samples of ten pooled embryos. One-way ANOVA with Holm-Sidak's multiple comparison test. At 72 hpf, *$P$<0.01 for control versus *cnr1*$^{-/-}$*; fabp10a:GFP* and **$P$<0.05 for control versus *cnr2*$^{-/-}$*; fabp10a:GFP*. Scale bars: 0.2 mm in A,B,D; 20 µm in E.

Development (2016) 143, 609-622 doi:10.1242/dev.121731

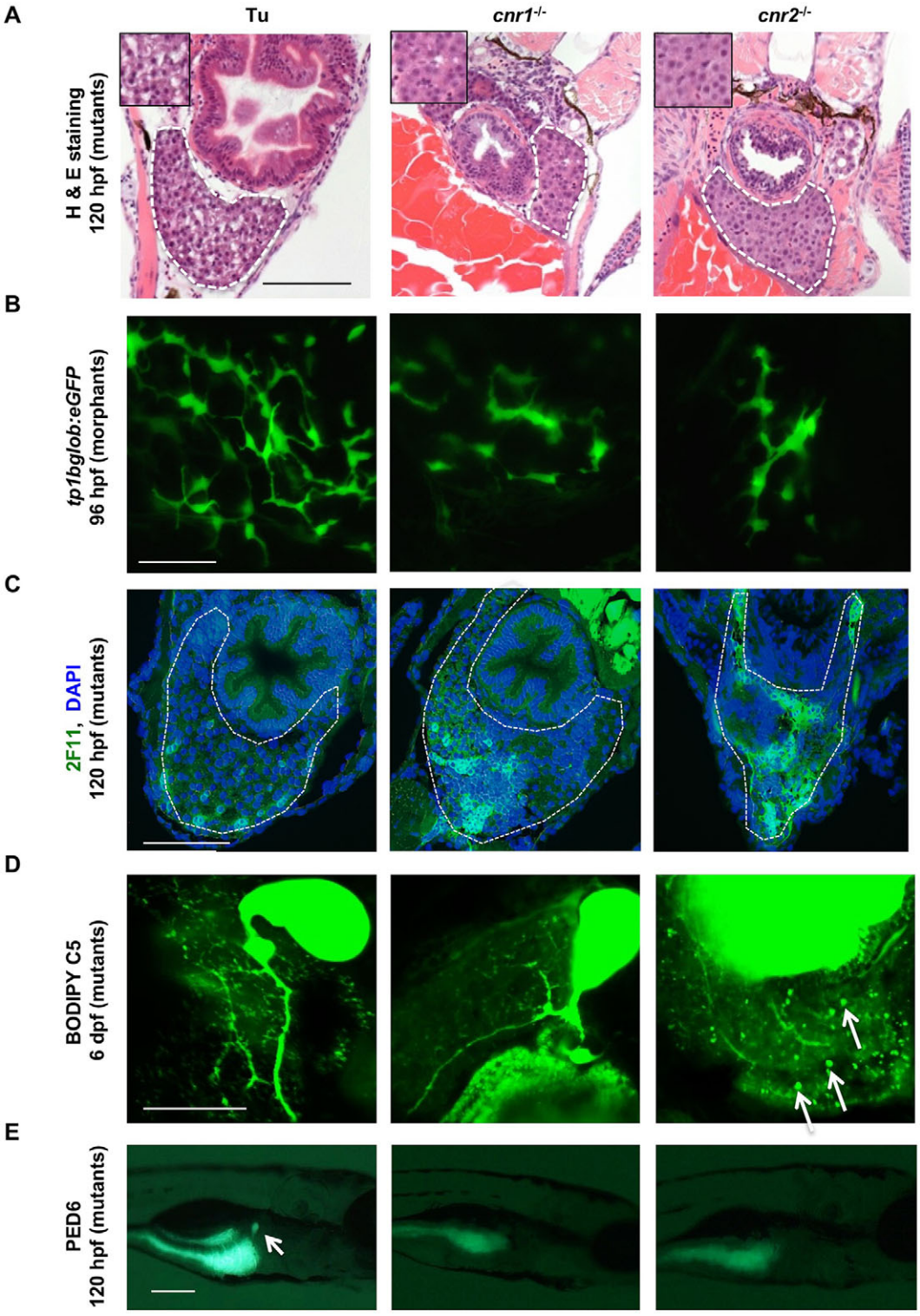


**Fig. 3. Livers in Cnr mutants eventually develop to normal size but continue to exhibit architectural and metabolic defects.** (A) H&E-stained transverse sections through 120 hpf larvae reveal altered hepatocyte morphology in *cnr1*$^{-/-}$ and *cnr2*$^{-/-}$ mutants, with more dense cytoplasm and decreased nucleus-to-cytoplasm ratios compared with WT, but no difference in hepatocyte size. Liver is outlined (white dashed line) and inset shows hepatocytes at higher magnification. (B) Confocal projections at 96 hpf in *cnr1* or *cnr2* morphants in the *tp1bglob:eGFP* Notch transgenic background, showing smaller liver size and decreased biliary branching and bile duct formation versus the control (6/10 *cnr1* morphants, 6/8 *cnr2* morphants). (C) Transverse sections of 120 hpf larvae stained with the biliary marker 2F11 and DAPI show an abnormal biliary tree in *cnr1*$^{-/-}$ (6/8 abnormal) and *cnr2*$^{-/-}$ (3/4 abnormal) livers. Liver region is outlined. (D) Confocal microscopy of livers in WT, *cnr1*$^{-/-}$ and *cnr2*$^{-/-}$ larvae at 6 dpf, showing metabolism of BODIPY C5 throughout the biliary tree. *cnr1*$^{-/-}$ larvae have decreased biliary branching ($n$=6/8 with phenotype of this representative image), while *cnr2*$^{-/-}$ livers are characterized by lipid deposits (arrows, $n$=7 /10 abnormal), as compared with WT (0/12). (E) PED6 lipase reporter assay in *cnr1*$^{-/-}$ ($n$=18/40 abnormal) and *cnr2*$^{-/-}$ ($n$=7/24 abnormal) mutants demonstrates decreased fluorescence compared with controls ($n$=0/24 abnormal) at 120 hpf. Fisher's exact test. *cnr1*$^{-/-}$ versus WT, $P$<0.0001; *cnr2*$^{-/-}$ versus WT, $P$=0.0094. Arrow marks the gallbladder, which does not fluoresce in the mutants. Scale bars: 0.1 mm in A,C; 20 µm in B,D; 0.2 mm in E.

Development (2016) 143, 609-622 doi:10.1242/dev.121731

(Fig. 3E). This disruption in lipid metabolism suggests that Cnr activity is necessary not only for hepatobiliary development, but also affects physiological regulation of metabolic homeostasis.

### *cnr1*$^{-/-}$ and *cnr2*$^{-/-}$ mutants demonstrate differential susceptibility to metabolic injury

To examine whether abnormal lipid handling during larval development alters susceptibility to pathological lipid accumulation, we utilized an established alcohol-induced steatosis model (Passeri et al., 2009): zebrafish exposed to 2% ethanol from 96-120 hpf develop steatosis at an incidence of 30-60%, as visualized by whole-mount Oil Red O (ORO) staining. *cnr1*$^{-/-}$, but not *cnr2*$^{-/-}$, mutants are protected from steatosis, with hepatic ORO staining detectable in only 19% of ethanol-exposed *cnr1*$^{-/-}$ larvae (Fig. S5A,B). These findings were confirmed by treatment with Cnr modulators (Fig. S5C) and in *cnr1* and *cnr2* morphants (Fig. S5D), and are consistent with reports on the differential role of Cnr in steatosis pathogenesis (Jeong et al., 2008; Louvet et al., 2011). Furthermore, *hand2*, a marker of zebrafish hepatic stellate cells, is usually upregulated in response to liver injury (Yin et al., 2012). Consistent with the ORO findings, *hand2* induction was observed in *cnr2*$^{-/-}$, but not *cnr1*$^{-/-}$, larvae at 120 hpf following ethanol exposure (Fig. S5E,F), consistent with the observed differential expression of *cnr1* and *cnr2* in different cell types.

To determine the impact of Cnr activity on the clinical problem of nutritionally induced hepatic steatosis, embryos were exposed to 3% egg yolk solution from 96-120 hpf, mimicking a high-fat diet. This treatment induces steatosis in ∼65% of WT larvae, but in only 24% of *cnr1*$^{-/-}$ larvae (Fig. S5G,H); similar to ethanol exposure, Cnr1 and Cnr2 modulation had opposing effects on egg yolk-induced steatosis (Fig. S5I). These findings imply that developmental disruption of EC signaling affects lipid homeostasis and susceptibility to metabolic insult, which may directly affect adult organ function.

### *cnr1*$^{-/-}$ and *cnr2*$^{-/-}$ mutants have altered metabolism in adulthood

To determine the long-term impact of the observed developmental and metabolic defects on organ homeostasis and lipid metabolism, adult mutant livers were examined. Levels of the endogenous Cnr ligands 2-AG and AEA were unaltered in liver tissue from *cnr1*$^{-/-}$ and *cnr2*$^{-/-}$ mutants compared with controls at 6 months, as determined by liquid chromatography/tandem mass spectrometry (Fig. S6A), consistent with findings in adult male *Cnr1* knockout mice (Mukhopadhyay et al., 2011). Ratios of liver mass to body mass in 6-month-old WT and *cnr1*$^{-/-}$ and *cnr2*$^{-/-}$ mutants were comparable (Fig. S6B). By contrast, liver histology revealed cholestasis and inflammatory infiltrates in *cnr1*$^{-/-}$ mutants. *cnr2*$^{-/-}$ mutants demonstrated abnormal cellular morphology with increased cytoplasm-to-nucleus ratio, suggesting spontaneous steatosis on a regular diet in the absence of metabolic injury induction (Fig. 4A), further indicating differential action of the receptors in different cell populations. Biliary marker expression was also severely diminished in *cnr1*$^{-/-}$ and *cnr2*$^{-/-}$ mutants, consistent with the embryonic biliary phenotype (Fig. 4B). To reveal systemic consequences of reduced Cnr activity and altered lipid metabolism, triglyceride levels were assessed in adult zebrafish serum, revealing significantly elevated levels in *cnr2*$^{-/-}$ mutants compared with age-matched *cnr1*$^{-/-}$ mutants and WT (Fig. 4C,D). The abnormal liver architecture and metabolism in adult Cnr mutants indicates that Cnr-regulated alterations in liver development and function can negatively impact adult homeostasis, causing ongoing disruptions in global lipid metabolism.

### Defects in EC signaling affect methionine metabolism

To define the metabolites most severely affected by disrupted EC signaling, we performed mass spectrometry-based metabolomic analysis on adult livers, detecting over 290 polar metabolites (Yuan et al., 2012). Metabolites clustered according to genotype without gender differences, indicating significant changes in individual metabolites from *cnr1*$^{-/-}$ and *cnr2*$^{-/-}$ livers. Methionine pathway intermediates were significantly altered: levels of methionine, homocysteine, S-adenosylhomocysteine, cysteine, homoserine, serine and S-adenosylmethionine were reduced (Fig. 5A, Fig. S6C,D), suggesting dysregulated methionine metabolism.

To further characterize the effects on methionine metabolism in *cnr1*$^{-/-}$ and *cnr2*$^{-/-}$ mutants, expression of key metabolic enzymes was examined by qRT-PCR at 120 hpf. *S-adenosylhomocysteine hydrolase* (*ahcy*) and *spermidine synthase* (*srm*) were downregulated in mutants, whereas *methylenetetrahydrofolate reductase* (*mthfr*) was upregulated (Fig. 5B). Analysis of RNA sequencing data from adult male *Cnr1* knockout mouse livers (Mukhopadhyay et al., 2011) revealed conserved downregulation of most methionine metabolism pathway enzymes (Fig. 5C). As methionine generates methyl groups for several physiological and molecular functions, we examined global protein methylation. Methylated protein levels, based on methyl-lysine detection, were diminished in *cnr1*$^{-/-}$ and *cnr2*$^{-/-}$ whole embryo lysates at 120 hpf (Fig. 5D). These data indicate dysregulated methionine metabolism in *cnr1*$^{-/-}$ and *cnr2*$^{-/-}$ mutants, which could be the direct result of loss of EC activity or a reflection of altered hepatocyte function.

### Methionine rescues liver development defects in Cnr mutants

To define a direct relationship between abnormal methionine metabolism and the observed liver phenotypes in *cnr1*$^{-/-}$ and *cnr2*$^{-/-}$ mutants, embryos were exposed to methionine metabolism intermediates. Treatment with methionine or cysteine, but not other amino acids (glycine, homocysteine), at physiological concentrations (100 µM) from 24-72 hpf rescued the liver size defect in *cnr1*$^{-/-}$ and *cnr2*$^{-/-}$ mutants as assessed by *fabp10a* ISH (Fig. 6A,B), while not affecting expression in controls. Methionine-treated *cnr1*$^{-/-}$ and *cnr2*$^{-/-}$ larvae demonstrated improved liver histology, with normal cytosol staining and decreased nucleus-to-cytoplasm ratios comparable to WT hepatocellular organization (Fig. 6C). To determine if methionine treatment likewise impacted lipid deposition and biliary morphogenesis, *cnr2*$^{-/-}$ mutants were treated with methionine beginning at 24 hpf, followed by administration of BODIPY C5 fluorophore at 6 dpf. Methionine-exposed *cnr2*$^{-/-}$ mutants exhibited increased biliary branching and improved lipid handling, with decreased fatty accumulation (Fig. 6D). Furthermore, treatment with methionine or cysteine protected *cnr2*$^{-/-}$ mutants, but not *cnr1*$^{-/-}$ or WT, from ethanol-induced steatosis (Fig. 6E,F). These findings indicate that early methionine supplementation can prevent many of the morphological hepatobiliary and metabolic defects seen with aberrant EC signaling.

To further corroborate that reduced methionine content negatively impacts liver development, we examined a previously characterized methionine metabolism disruption: Ahcy functions to break down S-adenosylhomocysteine into adenosine and homocysteine, and *ahcy* mutant zebrafish display hepatic steatosis and liver degeneration, followed by larval death (Matthews et al.,

Development (2016) 143, 609-622 doi:10.1242/dev.121731

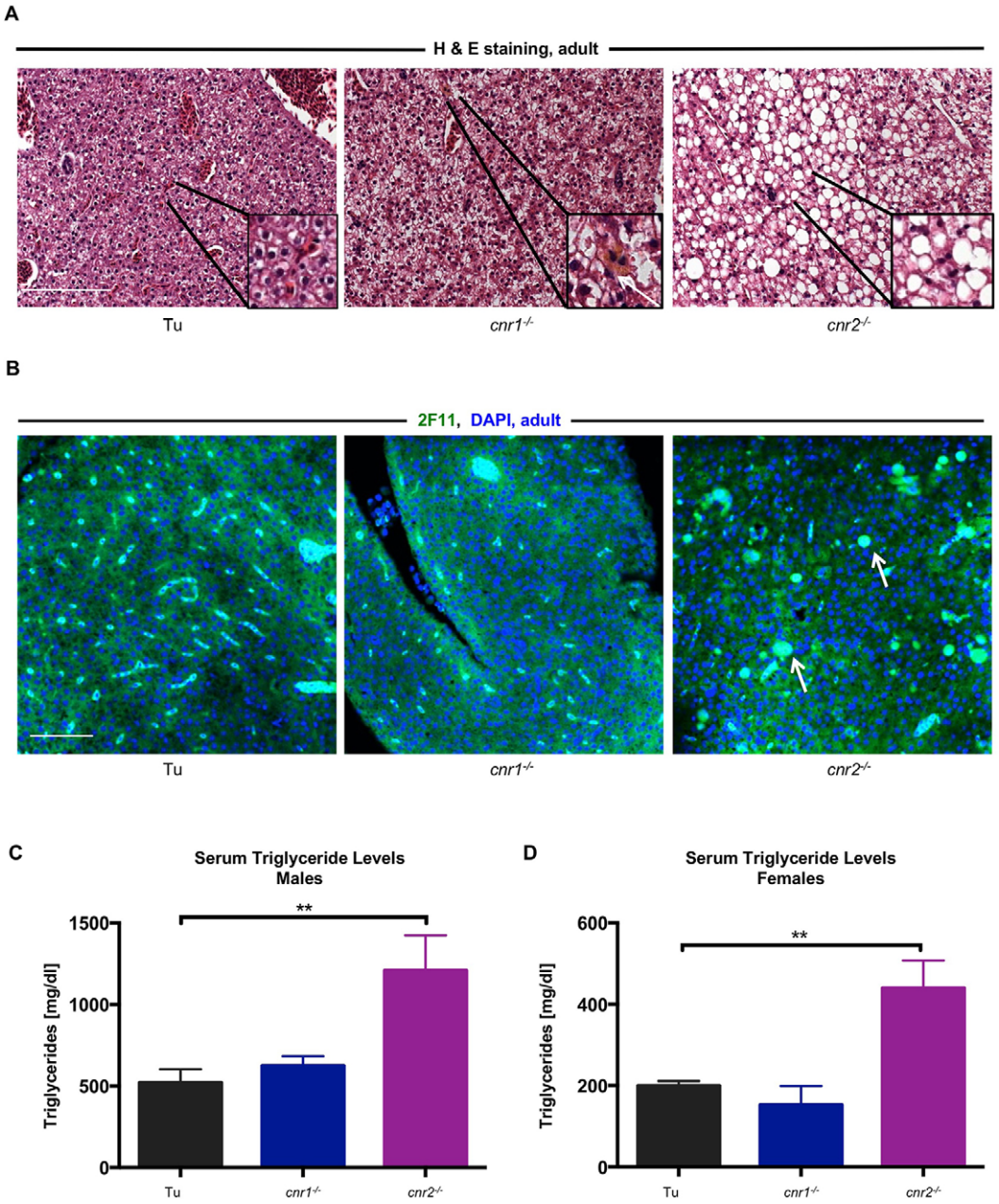


**Fig. 4. Metabolic dysregulation and aberrant histological features persist in adult Cnr mutants.** (A) H&E-stained adult liver sections show evidence of cholestasis (inset) and inflammatory infiltrates in *cnr1*$^{-/-}$ mutants. *cnr2*$^{-/-}$ mutants exhibit abnormal cellular morphology with increased open cytoplasm, suggesting extensive steatosis. (B) Adult liver sections stained for biliary marker 2F11 and with DAPI reveal decreased biliary tree formation in *cnr1*$^{-/-}$ mutants and cholestatic deposits (arrows) in *cnr2*$^{-/-}$ mutants. (C) Serum triglyceride content in male (C) and female (D) mutants. Adult *cnr2*$^{-/-}$ zebrafish have doubled triglyceride levels compared with WT and *cnr1*$^{-/-}$. Mean±s.e.m.; $n>5$. One-way ANOVA. **$P<0.01$ for WT versus *cnr2*$^{-/-}$. Scale bars: 0.1 mm.

2009). Morpholino knockdown of *ahcy* reduces liver size, as reflected in *fabp10a* expression, at 72 hpf. Exposure of morphants to methionine from 24-72 hpf rescued liver growth, demonstrating that disrupted methionine metabolism can directly impact liver development during hepatogenesis (Fig. S6E,F).

Finally, to determine the long-term impact of methionine exposure, *cnr2*$^{-/-}$ mutants were treated daily with methionine either until larval stages or for 2 months: with long-term intervention, liver histology was improved towards a WT appearance in H&E staining, as compared with untreated *cnr2*$^{-/-}$ controls or those exposed to methionine during embryonic stages alone, suggesting a lack of steatosis (Fig. 6G). These rescue studies indicate the important role of methionine in preventing histological and direct or subsequent metabolic consequences of *cnr2* loss.

### Srebfs mediate the effects of EC signaling

To identify potential mediators between methionine metabolism and EC signaling, we employed a candidate gene approach: prior studies in *C. elegans* showed that genes involved in one-carbon metabolism are regulated by Srebfs (Walker et al., 2011). Zebrafish homologs *srebf1* and *srebf2* are expressed in endoderm and developing liver beginning at 48 hpf, as determined by ISH and confirmed by qRT-PCR of FACS-sorted *fabp10a:GFP* hepatocytes (Fig. S6G-I). *srebf1* and *srebf2* expression, as determined by qRT-

Development (2016) 143, 609-622 doi:10.1242/dev.121731

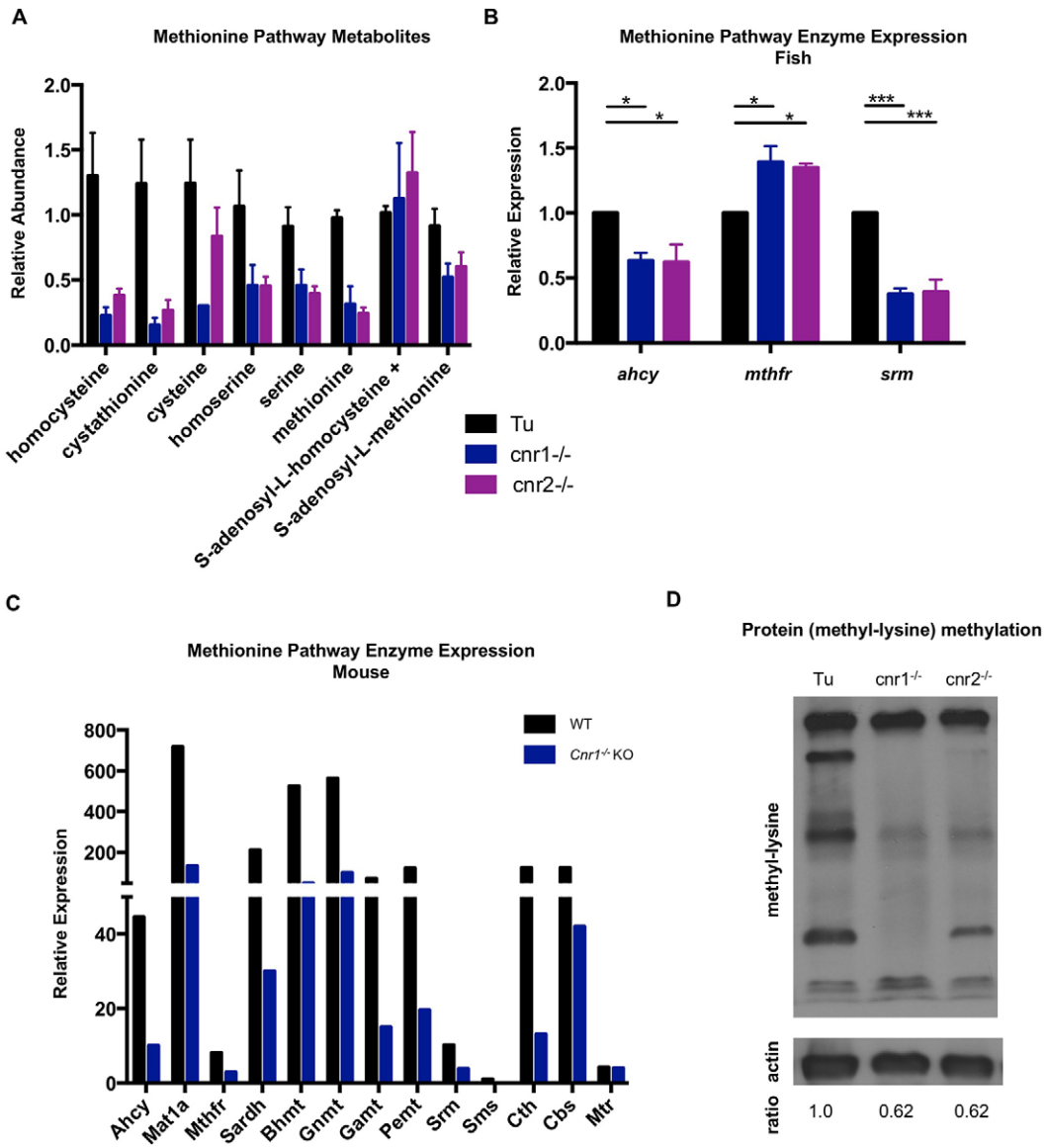


**Fig. 5. Polar metabolomics analysis reveals decreased levels of methionine metabolism intermediates in Cnr mutants.** (A) Methionine metabolism pathway intermediates are decreased in *cnr1*$^{-/-}$ and *cnr2*$^{-/-}$ adult female liver tissue. Mean±s.e.m.; *n*=3 biological samples. (B) Methionine metabolism enzymes are dysregulated in pooled 120 hpf *cnr1*$^{-/-}$ and *cnr2*$^{-/-}$ larvae: *ahcy* and *srm* are downregulated, whereas *mthfr* is upregulated. Mean±s.e.m.; *n*=3 pooled biological samples of 20 embryos each. One-way ANOVA. ***$P$<0.001 and *$P$<0.05 versus control. (C) RNA sequencing analysis reveals expression of methionine metabolism enzymes in male WT versus *Cnr1* knockout mice. *n*=6. (D) Western blot of methylated lysine in total protein from *cnr1*$^{-/-}$ and *cnr2*$^{-/-}$ larvae at 120 hpf shows a decreased and altered pattern of methylation in both mutants. Band intensity ratio of each mutant versus control is 0.62:1.

PCR, is downregulated in *cnr1*$^{-/-}$ and *cnr2*$^{-/-}$ mutants at 120 hpf and remains low in adult livers (Fig. 7A); low Srebf gene expression is also seen in *Cnr1*$^{-/-}$ male mouse livers (Fig. 7B), indicating conserved regulation by Cnr signaling. MO-mediated *srebf1* and *srebf2* knockdown decreased liver size at 72 hpf, which cannot be restored by Cnr agonists (Fig. S7A,B). By contrast, overexpression of *srebf1* and *srebf2* mRNA rescued *fabp10a* expression in *cnr1*$^{-/-}$ and *cnr2*$^{-/-}$ mutants (Fig. 7C,D), together indicating Srebf1/2 functions downstream of Cnr signaling. Further examination of mRNA-injected *cnr1*$^{-/-}$ and *cnr2*$^{-/-}$ larvae by H&E staining revealed that *srebf1*, but not *srebf2*, overexpression resulted in normalized liver histology, comparable to WT hepatocellular organization (Fig. S7C); these data suggest distinct roles of Srebf1 and Srebf2 targets in hepatic maturation. Additionally, overexpression of neither *srebf1* nor *srebf2* could rescue the aberrant BODIPY C5 lipid processing phenotypes of *cnr2*$^{-/-}$ larvae (Fig. S7D), probably owing to the non-cell-autonomous role of Cnr2 in hepatic development.

To further examine the direct relationship between Srebf and methionine in liver development, we examined their epistatic impact: methionine exposure did not rescue the liver size defects in Srebf morphants (Fig. S7E), probably owing to multiple downstream effects of Srebf during development. To delineate the dependence on methionine of Srebf-mediated rescue of liver defects in Cnr mutants, methionine synthesis was disrupted by *ahcy* knockdown in the context of Srebf overexpression: here, the Srebf-induced rescue of liver size in *cnr1*$^{-/-}$ and *cnr2*$^{-/-}$ embryos was inhibited (Fig. 7E-G). These modified epistatic analyses indicate that Srebf acts downstream of Cnr activity and upstream of methionine metabolism during liver development; however, the

Development (2016) 143, 609-622 doi:10.1242/dev.121731

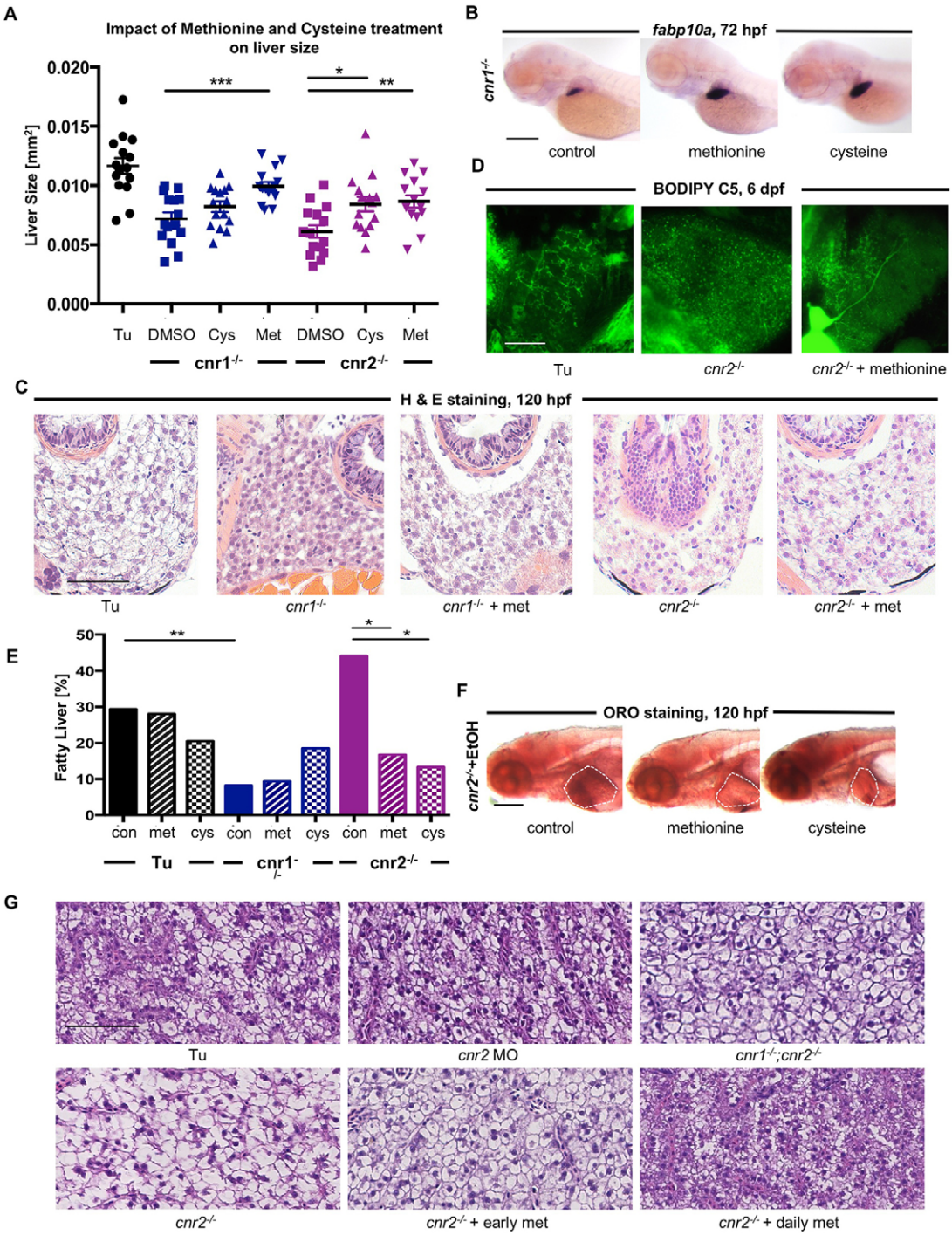


**Fig. 6. Treatment with methionine and cysteine can rescue liver development defects in Cnr mutants.** (A) Scatter plot of liver morphometric measurements of *cnr1*$^{-/-}$ and *cnr2*$^{-/-}$ mutants after 100 µM methionine or cysteine versus DMSO exposure from 24-72 hpf. Results shown represent one independent experiment of triplicate experiments yielding similar results. Mean±s.e.m.; $n$>15. One-way ANOVA. ***$P$<0.001, *cnr1*$^{-/-}$ methionine versus control; **$P$<0.01, *cnr2*$^{-/-}$ methionine versus control; *$P$<0.05, *cnr2*$^{-/-}$ cysteine versus control. (B) *fabp10a* expression at 72 hpf in *cnr1*$^{-/-}$ embryos after DMSO, methionine or cysteine exposure from 24-72 hpf. (C) H&E staining of transverse sections of 120 hpf larvae shows that treatment of *cnr1*$^{-/-}$ and *cnr2*$^{-/-}$ mutants with methionine partially restores WT liver histology. *cnr1*$^{-/-}$, 6 abnormal/9; *cnr1*$^{-/-}$+methionine, 5 normal/7; $P$=0.065 (Chi-square). *cnr2*$^{-/-}$, 6 abnormal/9; *cnr2*$^{-/-}$+methionine, 6 normal/8; $P$=0.043 (Chi-square). (D) Confocal microscopy images of livers in *cnr2*$^{-/-}$ larvae after BODIPY C5 incorporation with and without methionine treatment. Extensive biliary branching is observed in WT larvae, and decreased branching with lipid and cholestatic deposition in *cnr2*$^{-/-}$ mutants (7 abnormal/10). Treatment of *cnr2*$^{-/-}$ mutants with methionine causes increased biliary branching and decreased lipid accumulation (2 abnormal/6). (E) Percentage of larvae with fatty liver after ethanol-induced liver injury and with methionine or cysteine treatment for *cnr1*$^{-/-}$ and *cnr2*$^{-/-}$ larvae at 120 hpf. $n$>30 samples. Fisher's exact test. *$P$<0.05 and **$P$<0.01 for methionine and cysteine versus DMSO. (F) ORO stain in *cnr2*$^{-/-}$ embryos at 120 hpf after 2% ethanol exposure alone or co-treated with 100 µM methionine or cysteine from 96-120 hpf. Liver region is outlined. (G) H&E staining of liver sections in 2-month-old male zebrafish. *cnr2* morphant liver histology appears similar to that of WT; *cnr2*$^{-/-}$ and *cnr1*$^{-/-}$*; cnr2*$^{-/-}$ double mutants have decreased cytoplasmic hepatocyte staining. Early methionine treatment of *cnr2*$^{-/-}$ mutants had no effect on liver histology; however, daily methionine altered histological appearance towards WT features, with increased cytoplasmic staining and decreased cytoplasm-to-nucleus ratios. $n$=5/group. Scale bars: 0.2 mm in B,F; 0.1 mm in C; 20 µm in D; 50 µm in G.

Development (2016) 143, 609-622 doi:10.1242/dev.121731

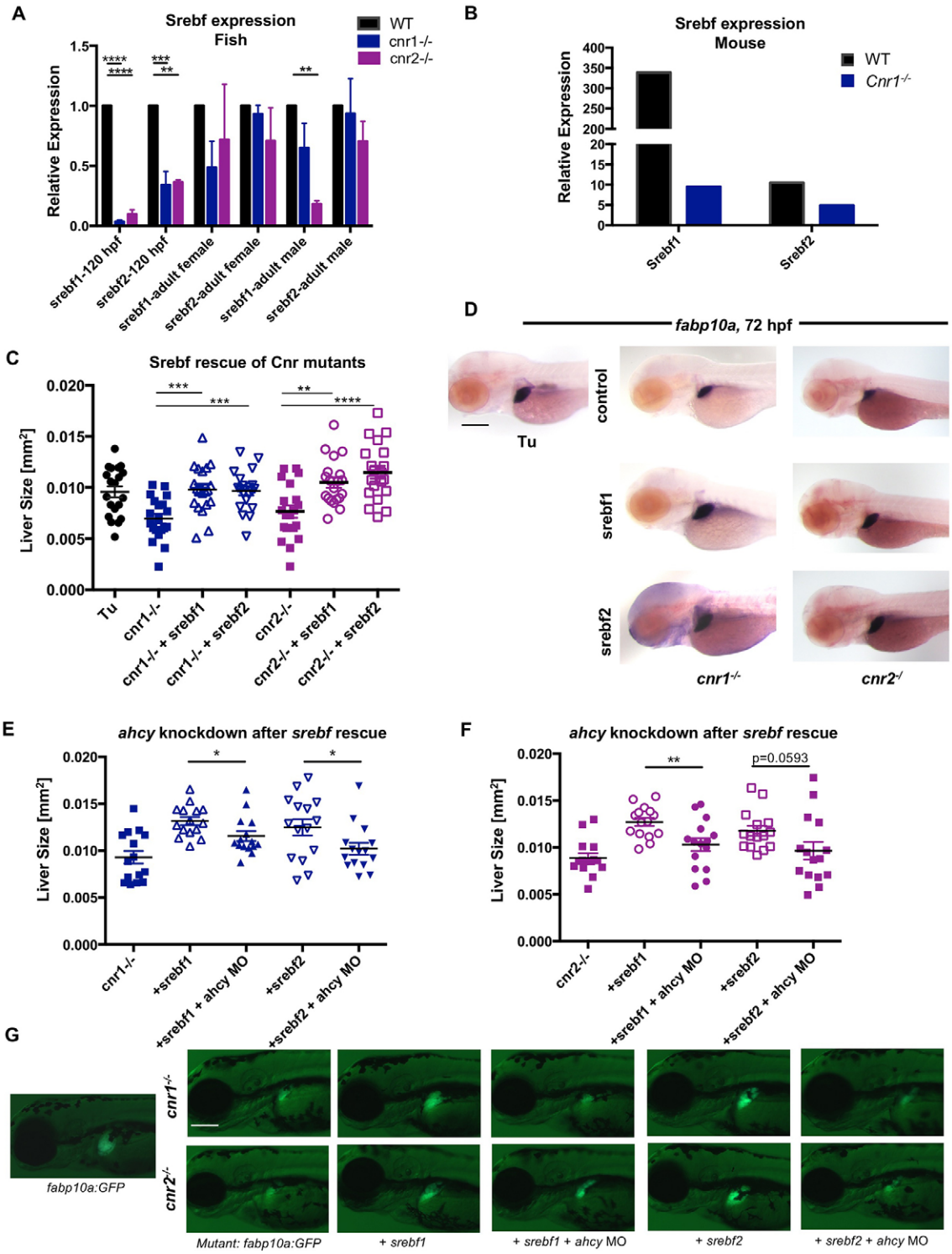


**Fig. 7. EC signaling regulates methionine metabolism via Srebfs in Cnr mutants.** (A) *srebf1* and *srebf2* expression in pooled WT, *cnr1*$^{-/-}$ and *cnr2*$^{-/-}$ zebrafish embryos at 120 hpf, and in adult livers, quantified by qRT-PCR. Data analyzed using the ΔΔCt method. Mean±s.e.m.; *n*=3 pooled biological samples of 20 embryos each. One-way ANOVA. ****$P$<0.0001, ***$P$<0.001 and **$P$<0.01 for *srebf1* or *srebf2* expression in mutants versus WT. (B) *Srebf1* and *Srebf2* expression in male *Cnr1*$^{-/-}$ mice. *n*=6. (C,D) Scatter plot of liver morphometric measurements (C) and *fabp10a* ISH (D) at 72 hpf in *cnr1*$^{-/-}$ and *cnr2*$^{-/-}$ mutants with and without overexpression of *srebf1* and *srebf2* mRNA. Results shown represent one independent experiment of triplicate experiments which yielded similar results. Mean±s.e.m.; *n*>15. One-way ANOVA. ***$P$<0.001 for *cnr1*$^{-/-}$ control versus *srebf1* or *srebf2* overexpression; **$P$<0.01 for *cnr2*$^{-/-}$ control versus *srebf1* overexpression; ****$P$<0.0001 for *cnr2*$^{-/-}$ control versus *srebf2* overexpression. (E-G) Scatter plot of liver morphometric measurements (E,F) and live imaging (G) of *cnr1*$^{-/-}$*; fabp10a:GFP* and *cnr2*$^{-/-}$*; fabp10a:GFP* at 72 hpf with overexpression of *srebf1* and *srebf2* in the presence and absence of concurrent *ahcy* morpholino knockdown. Results represent one independent experiment of triplicate experiments yielding similar results. Mean±s.e.m.; *n*>15. Student's *t*-test. *$P$<0.05 in *cnr1*$^{-/-}$ background (E); **$P$<0.01 in *cnr2*$^{-/-}$ background (F). Scale bars: 0.2 mm.

Development (2016) 143, 609-622 doi:10.1242/dev.121731

inability to reach linear correspondence across all assays suggests that Cnr and Srebf have additional downstream mediators and targets that are independent of methionine and that contribute to the complex hepatobiliary maturation and metabolic phenotypes.

## DISCUSSION

In this study, we characterize the requirement for Cnr1 and Cnr2 activity in normal zebrafish liver development and function. Cnr loss impairs hepatocyte differentiation and proliferation and alters biliary development and function, but spares earlier stages of endoderm specification. Even though *cnr1* and *cnr2* are expressed in different liver cell types at 72 hpf, EC signaling is required for the establishment and maintenance of proper hepatic physiology and lipid metabolism during embryogenesis. Srebfs and methionine act downstream of Cnr signaling and are responsible for several of the phenotypes observed in $cnr1^{-/-}$ and $cnr2^{-/-}$ mutants. This important interaction demonstrates a novel role for EC signaling during liver development that has functional consequences for metabolic homeostasis in the adult organ.

### EC signaling through Cnr is required for normal liver development

Our results demonstrate that the lack of a normal hepatocyte population during hepatogenesis impedes proper liver physiology throughout life. Although important for optimal liver function, *cnr1* and *cnr2* are not essential, as $cnr1^{-/-}; cnr2^{-/-}$ double mutants reach adulthood and are fertile. EC signaling has previously been implicated in promoting trophoblast cell lineage differentiation (Sun et al., 2010) and neural development (Palazuelos et al., 2012; Psychoyos et al., 2012); one indication that Cnr signaling may also affect endodermal development and/or metabolic function was observed in $Cnr1^{-/-}$ *ob/ob* double-mutant mice, which exhibit growth retardation and exacerbated glucose intolerance (Li et al., 2013). The developmental phenotypes observed in Cnr mutant zebrafish support previously described liver abnormalities in Cnr knockout mice: the impact of Cnr activity on embryonic liver maturation might explain the delayed or aberrant hepatocyte proliferation and recovery of liver mass seen after partial hepatectomy in adult *Cnr1* and *Cnr2* knockout mice (Teixeira-Clerc et al., 2010), as the recapitulation of proliferation-promoting developmental pathways has been shown to be important during liver regeneration (Goessling et al., 2008; Nissim et al., 2014; Yin et al., 2012).

Our findings shed new insights into common metabolic diseases such as hepatic steatosis, obesity and diabetes, which have complex genetic causes. Patients with genetic variants or deficiencies of *CNR1*, *CNR2*, the enzyme fatty acid amide hydrolase (*FAAH*), which breaks down ECs, and methionine metabolism enzymes such as *AHCY*, *PEMT*, *GNMT*, *MTHFR* and *CBS*, have a higher likelihood of developing metabolic abnormalities or liver disease (Baric et al., 2004; Coppola et al., 2014; Feng et al., 2010; Floreani et al., 2010; Mato et al., 2008; Sipe et al., 2005). Our work provides evidence that the developmental defect itself and/or a persisting metabolic abnormality may significantly impact adult liver homeostasis. These findings offer therapeutic opportunities for early or long-term interventions that might minimize disease phenotypes later in life. For example, modulation of peripheral Cnr alone can impact nutrient utilization and response to excessive nutrient overload, and prior studies have utilized the Cnr1 antagonist rimonabant for obesity treatment. Our studies further suggest that normal Cnr2 activity, present not in hepatocytes but in another liver cell population, is likewise important for optimal liver and metabolic function.

### Importance of methionine for development and hepatic function

Methionine metabolism generates S-adenosylmethionine (SAMe), which is required for multiple cellular functions, including as a methyl donor for nucleic acid, phospholipid, and protein methylation processes during epigenetic regulation. Methionine is also crucial for protein synthesis as an amino acid, and is therefore essential for cellular proliferation and function. Mammalian models for studying methionine metabolism enzymes also reveal the importance of this pathway for early development: knockout of methionine synthase (*Mtr*) leads to post-implantation embryonic death, while loss of *Mthfr* causes smaller body size and growth retardation (Chen et al., 2001; Swanson et al., 2001). Correlations between diet and environmental exposure leading to long-term metabolic dysregulation are established in mammals, with maternal diet impacting DNA methylation in offspring (Ozanne, 2014). Specifically, reducing methionine in the mammalian diet disrupts proper DNA methylation, leading to increased adiposity (Sinclair et al., 2007), while lack of proper embryonic nutrition can lead to DNA methylation defects and aberrant adult metabolism (Radford et al., 2014). Even paternal diet low in protein can affect cytosine methylation and gene expression in the mouse embryo, impacting hepatic lipid metabolism, including Srebf function (Carone et al., 2010). The developmental and adult phenotypes observed in the Cnr mutants might at least in part be mediated by abnormalities in methionine metabolism during development.

Methionine metabolism enzymes are primarily expressed in the liver, and abnormal methionine metabolism has been linked to hepatic steatosis: a methionine-choline-deficient diet has long been associated with hepatic steatosis in mouse models (Best et al., 1936). Zebrafish *ahcy* mutants, defective in metabolizing S-adenosylhomocysteine into adenosine and homocysteine, exhibit steatosis and liver degeneration (Matthews et al., 2009), while mouse knockouts for the *Mat1a*, *Pemt*, *Gnmt*, *Cbs* and *Mthfr* enzymes develop steatohepatitis and hepatocellular carcinoma, potentially via decreased methylation or AMP-activated protein kinase inhibition (Mato et al., 2008). Intriguingly, SAMe supplementation appears to prevent hepatocellular carcinoma in rodent models (Pascale et al., 1992). Our long-term methionine treatment of $cnr2^{-/-}$ mutants improves histological abnormalities, further emphasizing the importance of proper methionine levels for hepatic structure and function.

### EC signaling regulates methionine metabolism via Srebfs

Cnr1 and Cnr2 are G-protein coupled receptors that inhibit adenylyl cyclase and decrease cyclic AMP levels while stimulating MAP kinase, resulting in downstream activation of the ERK, FAK, JNK or PI3K/AKT pathways to control cell fate (McAllister and Glass, 2002; Pagotto et al., 2006). Although methionine adenosyltransferase (Mat1a) can regulate ERK and PI3K/AKT (Chen et al., 2004; Frau et al., 2013; Tomasi et al., 2010), these pathways have additional upstream activators besides ECs, and a direct relationship between Cnr signaling and methionine metabolism has not previously been established. Srebfs are established downstream targets of EC signaling (Jeong et al., 2008). Although defects in EC signaling or methionine metabolism components are independently associated with hepatic steatosis, fibrosis or liver cancer (Huang et al., 2011; Mato et al., 2008; Pisanti et al., 2013), here we highlight a previously unknown pathway between EC signaling, Srebf and methionine metabolism that impacts liver development and function. Further studies are necessary to define the cell types involved and whether this

Development (2016) 143, 609-622 doi:10.1242/dev.121731

regulation involves autocrine, paracrine or other signaling mechanisms.

Srebfs promote fatty acid and cholesterol uptake and synthesis and can act downstream of EC signaling in the liver, with levels that can be regulated in zebrafish and mice by administration of the EC anandamide (Migliarini and Carnevali, 2008; Pai et al., 2013). In mice, modulation of dietary methionine can alter Srebf expression by feedback induction (Aissa et al., 2014). Similarly, expression of methionine metabolism genes in *C. elegans* not only depends on SREBF1 (SBP-1), but also feeds back to control SREBF1 and affect lipid metabolism (Walker et al., 2011). In our studies, overexpression of *srebf1* and *srebf2* in *cnr1*$^{-/-}$ and *cnr2*$^{-/-}$ zebrafish embryos restores normal liver size. However, whereas liver growth could be rescued in Cnr mutants with methionine, this was not possible in *srebf1* and *srebf2* morphants. This is likely to indicate that the impact of Srebf knockdown goes beyond methionine regulation. Srebfs can directly regulate virtually all enzymes involved in the biosynthesis of cholesterol (Horton et al., 2003), which, among other functions, is a central component of cell membranes and required for cell proliferation. This conclusion is also supported by the complete or partial embryonic lethality of Srebf knockout mice (Shimano et al., 1997). However, our epistatic analysis performed in the context of Srebf overexpression demonstrates a dependence on methionine metabolism downstream of Srebf to mediate the effect of Cnr signaling on liver development.

In summary, in an unbiased screen for novel regulators of liver development in zebrafish we have uncovered pathways that can reveal insights into developmental metabolism and adult liver homeostasis with implications for mammalian species. We define a novel role for EC signaling that integrates and coordinates the organism's metabolic needs by regulating appetite in the CNS, while also promoting liver proliferation and metabolic function, achieved in part through the regulation of methionine metabolism.

## MATERIALS AND METHODS

### Zebrafish husbandry

Zebrafish were maintained according to standard Institutional Animal Care and Use Committee guidelines.

### Generation of *cnr1*$^{-/-}$ and *cnr2*$^{-/-}$ mutants

TALE repeat arrays (designed using ZiFiT Targeter, http://zifit.partners.org/ZiFiT/) targeting *cnr1* and *cnr2* genes using the REAL system were cloned into TALEN vectors (Sander et al., 2011). TALEN mRNA pairs were injected into one-cell stage Tubingen (Tu) WT embryos, and somatic mutation rates from pooled embryos were analyzed. Adult founders were identified by assessing clutches for heterozygous progeny. Heterozygotes were raised to adulthood, genotyped, and outcrossed for at least three generations to reduce TALEN off-target effects.

### *In situ* hybridization

ISH was conducted on paraformaldehyde-fixed embryos using standard protocols (Thisse and Thisse, 2008). Probes for *srebf1* and *srebf2* were generated as described in the supplementary Materials and Methods. Changes in *fabp10a*, *sid4*, *gc*, *tfa*, *hhex*, *foxa3*, *prox1* and *fabp2* expression were scored using ImageJ (NIH) to quantify liver, endoderm or progenitor population size in images. ANOVA was conducted for comparison of liver sizes across multiple groups. *cnr1*, *cnr2*, *hand2*, *srebf1* and *srebf2* expression patterns were assessed throughout development. Other expression patterns were scored as 'small', 'normal' or 'large' within a population distribution, consistent with the quantitative size distribution. The percentage of the total population that was altered was calculated for each genotype/treatment group.

### Fluorescence-activated cell sorting

*fabp10a:GFP* embryos were incubated in 50 µg/ml liberase (Roche) at 37°C for 1.5 h, manually dissociated, and strained through a 35 µm nylon mesh filter. For cell quantification, GFP$^{+}$ cells were counted using a BD FACSAria II flow cytometer. For cell sorting, GFP$^{+}$ and GFP$^{-}$ fractions were separated using a BD FACSAria II SORP flow cytometer (Goessling et al., 2008).

### qRT-PCR

RNA extracted from pooled embryos or adult livers using Trizol was treated using the TURBO DNA-free DNase kit (Life Technologies); cDNA was generated using iScript cDNA synthesis reagents (Bio-Rad). Cells isolated by FACS (~200,000) were processed using the RNAqueous-Micro Total RNA Isolation Kit (Thermo Fisher) according to the manufacturer's protocol. Amplified cDNA was prepared using the Ovation Pico WTA System V2 (NuGEN). All qRT-PCR was performed using SYBR Green Supermix (Bio-Rad) and relative expression levels were calculated using the ΔΔCt method. Primers are listed in Table S1.

### EdU incorporation and TUNEL staining

EdU incorporation was conducted using the Click-iT Plus EdU Alexa Fluor 647 Flow Cytometry and Imaging Kit (Life Technologies). Embryos were incubated on ice for 10 min, then incubated with 400 µM EdU for 2 h at 28°C, and labeled following the manufacturer's protocol. EdU-positive cells were visualized by confocal microscopy or processed using the above cell sorting procedure. TUNEL staining for apoptotic cells is described in the supplementary Materials and Methods.

### Morpholino injection

ATG and splice-blocking morpholino oligonucleotides (GeneTools) were designed against *cnr1*, *cnr2*, *srebf1*, *srebf2* and *ahcy*. The *cnr1*, *cnr2* and *ahcy* splice-blocking morpholinos were previously validated (Esain et al., 2015; Matthews et al., 2009). Injections were performed at the one-cell stage, with a mismatch standard morpholino used for control. Morpholino sequences, injected concentrations and amounts are listed in Table S2.

### Chemical exposure

Chemicals used are listed in Table S3 and were utilized at the indicated concentrations.

### Oil Red O staining

Whole-mount Oil Red O staining was conducted as previously described (Passeri et al., 2009). Embryos were scored based on the presence of red lipid droplets in the liver. Fisher's exact test was used to compare changes in liver phenotype.

### Histology and immunohistochemistry

Adult zebrafish midsections and embryos were processed for Hematoxylin and Eosin (H&E) staining using standard protocols, and examined together with Dr Jason Hornick, a board-certified pathologist. Immunohistochemistry was performed using 2F11 antibody and FITC fluorescent secondary antibody (see Table S4).

### Analysis of lipid metabolism in live zebrafish embryos

Embryos were exposed to 0.1 µg/ml PED6 (Farber, 2001) at 12 hpf for 6 h, washed, and then imaged by fluorescence microscopy. BODIPY C5 fluorophore (Invitrogen) was utilized to observe lipid metabolism and digestive organ morphology *in vivo*. Embryos were incubated in 6.4 µM BODIPY C5 in 5% egg yolk solution at 6 dpf for 4 h, followed by confocal microscopy.

### Serum lipid tests

Adult zebrafish blood was collected by tail incision (Babaei et al., 2013). Serum triglyceride and cholesterol concentrations were analyzed using microplate-based enzyme activity kits (Pointe Scientific).

Development (2016) 143, 609-622 doi:10.1242/dev.121731

### Polar metabolomics

Quantitative polar metabolomics profiling was performed after extraction from zebrafish livers on AB/SCIEX 5000 QTRAP LC/MS/MS instrumentation, using previously described protocols (Yuan et al., 2012).

### EC measurements

The tissue levels of ECs were measured as described in the supplementary Materials and Methods.

### Western blotting

Proteins extracted from pooled larvae populations at 120 hpf were resolved using SDS-PAGE, and methylated lysine was detected with specific primary antibody and HRP-conjugated secondary antibody, as listed in Table S4.

### mRNA injection

*srebf1* and *srebf2* were amplified from WT zebrafish cDNA using the primers (5′-3′): *srebf1*, AAGAGCATCCGAGGACAATG and GTGTTCAGGTGGATGTGACG; *srebf2*, TGTGAGTGAACGAGGAGACG and GTTATGATGCAGCGTTGGTG. Polyadenylated mRNA was transcribed using the mMESSAGE mMACHINE Transcription Kit (Ambion), and injected into one-cell stage zebrafish embryos at 100 pg/nl.

#### Acknowledgements

We thank Dr Jason Hornick for histopathological analysis; Dr John Asara for metabolomics assessment; Dr Ruma Banerjee for helpful discussions; and staff of the Beth-Israel Deaconess Medical Center Zebrafish Facility for zebrafish husbandry.

#### Competing interests

The authors declare no competing or financial interests.

#### Author contributions

L.Y.L. and W.G. conceived and designed the experiments and analyzed the data. L.Y.L. performed all zebrafish experiments. T.E.N. and W.G. conducted the original chemical screen. K.A. generated ISH probes and performed ISH. M.C. and L.Y.L. performed FACS quantification. M.C. and S.S.-B. conducted FACS sorting and qRT-PCR. A.J.K. conducted treatments of adult zebrafish. B.M., R.C. and G.K. performed EC measurements and shared mouse RNA sequencing data. L.Y.L. and W.G. wrote the manuscript. All authors reviewed and edited the manuscript.

#### Funding

This work was supported by National Institutes of Health NIAAA [F31AA022548 to L.Y.L.] and NIDDK [R03096156 to T.E.N. and R01DK090311 to W.G.], and by the Harvard Stem Cell Institute [to T.E.N. and W.G.]. W.G. is a Pew Scholar in the Biomedical Sciences. Deposited in PMC for release after 12 months.

#### Supplementary information

Supplementary information available online at
http://dev.biologists.org/lookup/suppl/doi:10.1242/dev.121731/-/DC1

#### References

**Aissa, A. F., Tryndyak, V., de Conti, A., Melnyk, S., Gomes, T. D. U. H., Bianchi, M. L. P., James, S. J., Beland, F. A., Antunes, L. M. G. and Pogribny, I. P.** (2014). Effect of methionine-deficient and methionine-supplemented diets on the hepatic one-carbon and lipid metabolism in mice. *Mol. Nutr. Food Res.* **58**, 1502-1512.

**Babaei, F., Ramalingam, R., Tavendale, A., Liang, Y., Yan, L. S. K., Ajuh, P., Cheng, S. H. and Lam, Y. W.** (2013). Novel blood collection method allows plasma proteome analysis from single zebrafish. *J. Proteome Res.* **12**, 1580-1590.

**Baric, I., Fumic, K., Glenn, B., Cuk, M., Schulze, A., Finkelstein, J. D., James, S. J., Mejaski-Bosnjak, V., Pazanin, L., Pogribny, I. P. et al.** (2004). S-adenosylhomocysteine hydrolase deficiency in a human: A genetic disorder of methionine metabolism. *Proc. Natl. Acad. Sci. USA* **101**, 4234-4239.

**Best, C. H., Mawson, M. E., McHenry, E. W. and Ridout, J. H.** (1936). The effect of diets low in choline. *J. Physiol. (Lond.)* **86**, 315-322.

**Carone, B. R., Fauquier, L., Habib, N., Shea, J. M., Hart, C. E., Li, R., Bock, C., Li, C., Gu, H., Zamore, P. D. et al.** (2010). Paternally induced transgenerational environmental reprogramming of metabolic gene expression in mammals. *Cell* **143**, 1084-1096.

**Carten, J. D., Bradford, M. K. and Farber, S. A.** (2011). Visualizing digestive organ morphology and function using differential fatty acid metabolism in live zebrafish. *Dev. Biol.* **360**, 276-285.

**Castillo, P. E., Younts, T. J., Chávez, A. E. and Hashimotodani, Y.** (2012). Endocannabinoid signaling and synaptic function. *Neuron* **76**, 70-81.

**Chen, Z., Karaplis, A. C., Ackerman, S. L., Pogribny, I. P., Melnyk, S., Lussier-Cacan, S., Chen, M. F., Pai, A., John, S. W. M., Smith, R. S. et al.** (2001). Mice deficient in methylenetetrahydrofolate reductase exhibit hyperhomocysteinemia and decreased methylation capacity, with neuropathology and aortic lipid deposition. *Hum. Mol. Genet.* **10**, 433-443.

**Chen, L. Zeng, Y., Lee, T. D., French, S. W., Corrales, F. J., Garcia-Trevijano, E. R., Avila, M. A., Mato, J. M. and Lu, S. C.** (2004). Impaired liver regeneration in mice lacking methionine adenosyltransferase 1A. *FASEB J.* **18**, 914-916.

**Coppola, N., Zampino, R., Bellini, G., Macera, M., Marrone, A., Pisaturo, M., Boemio, A., Nobili, B., Pasquale, G., Maione, S. et al.** (2014). Association between a polymorphism in cannabinoid receptor 2 and severe necroinflammation in patients with chronic hepatitis C. *Clin. Gastroenterol. Hepatol.* **12**, 334-340.

**Devane, W., Hanus, L., Breuer, A., Pertwee, R., Stevenson, L., Griffin, G., Gibson, D., Mandelbaum, A., Etinger, A. and Mechoulam, R.** (1992). Isolation and structure of a brain constituent that binds to the cannabinoid receptor. *Science* **258**, 1946-1949.

**Esain, V., Kwan, W., Carroll, K. J., Cortes, M., Liu, S. Y., Frechette, G. M., Sheward, L. M. V., Nissim, S., Goessling, W. and North, T. E.** (2015). Cannabinoid receptor-2 regulates embryonic hematopoietic stem cell development via prostaglandin E2 and P-selectin activity. *Stem Cells* **33**, 2596-2612.

**Farber, S. A.** (2001). Genetic analysis of digestive physiology using fluorescent phospholipid reporters. *Science* **292**, 1385-1388.

**Feng, Q., Jiang, L., Berg, R. L., Antonik, M., MacKinney, E., Gunnell-Santoro, J., McCarty, C. A. and Wilke, R. A.** (2010). A common CNR1 (cannabinoid receptor 1) haplotype attenuates the decrease in HDL cholesterol that typically accompanies weight gain. *PLoS ONE* **5**, e15779.

**Floreani, A., Lazzari, R., Macchi, V., Porzionato, A., Variola, A., Colavito, D., Leon, A., Guido, M., Baldo, V., De Caro, R. et al.** (2010). Hepatic expression of endocannabinoid receptors and their novel polymorphisms in primary biliary cirrhosis. *J. Gastroenterol.* **45**, 68-76.

**Frau, M., Feo, F. and Pascale, R. M.** (2013). Pleiotropic effects of methionine adenosyltransferases deregulation as determinants of liver cancer progression and prognosis. *J. Hepatol.* **59**, 830-841.

**Garnaas, M. K., Cutting, C. C., Meyers, A., Kelsey, P. B., Harris, J. M., North, T. E. and Goessling, W.** (2012). Rargb regulates organ laterality in a zebrafish model of right atrial isomerism. *Dev. Biol.* **372**, 178-189.

**Goessling, W., North, T. E., Lord, A. M., Ceol, C., Lee, S., Weidinger, G., Bourque, C., Strijbosch, R., Haramis, A.-P., Puder, M. et al.** (2008). APC mutant zebrafish uncover a changing temporal requirement for wnt signaling in liver development. *Dev. Biol.* **320**, 161-174.

**Horton, J. D., Shah, N. A., Warrington, J. A., Anderson, N. N., Park, S. W., Brown, M. S. and Goldstein, J. L.** (2003). Combined analysis of oligonucleotide microarray data from transgenic and knockout mice identifies direct SREBP target genes. *Proc. Natl. Acad. Sci. USA* **100**, 12027-12032.

**Huang, L., Quinn, M. A., Frampton, G. A., Golden, L. E. and DeMorrow, S.** (2011). Recent advances in the understanding of the role of the endocannabinoid system in liver diseases. *Dig. Liver Dis.* **43**, 188-193.

**Jeong, W.-I., Osei-Hyiaman, D., Park, O., Liu, J., Bátkai, S., Mukhopadhyay, P., Horiguchi, N., Harvey-White, J., Marsicano, G., Lutz, B. et al.** (2008). Paracrine activation of hepatic CB1 Receptors by stellate cell-derived endocannabinoids mediates alcoholic fatty liver. *Cell Metab.* **7**, 227-235.

**Julien, B., Grenard, P., Teixeira-Clerc, F., Van Nhieu, J. T., Li, L., Karsak, M., Zimmer, A., Mallat, A. and Lotersztajn, S.** (2005). Antifibrogenic role of the cannabinoid receptor CB2 in the liver. *Gastroenterology* **128**, 742-755.

**Lam, C. S., Rastegar, S. and Strähle, U.** (2006). Distribution of cannabinoid receptor 1 in the CNS of zebrafish. *Neuroscience* **138**, 83-95.

**Li, Z., Schmidt, S. F. and Friedman, J. M.** (2013). Developmental role for endocannabinoid signaling in regulating glucose metabolism and growth. *Diabetes* **62**, 2359-2367.

**Louvet, A., Teixeira-Clerc, F., Chobert, M.-N., Deveaux, V., Pavoine, C., Zimmer, A., Pecker, F., Mallat, A. and Lotersztajn, S.** (2011). Cannabinoid CB2 receptors protect against alcoholic liver disease by regulating Kupffer cell polarization in mice. *Hepatology* **54**, 1217-1226.

**Maccarrone, M., Gasperi, V., Catani, M. V., Diep, T. A., Dainese, E., Hansen, H. S. and Avigliano, L.** (2010). The endocannabinoid system and its relevance for nutrition. *Annu. Rev. Nutr.* **30**, 423-440.

**Martin, B. R.** (2006). Pharmacological characterization of novel water-soluble cannabinoids. *J. Pharmacol. Exp. Ther.* **318**, 1230-1239.

**Mato, J. M., Martínez-Chantar, M. L. and Lu, S. C.** (2008). Methionine metabolism and liver disease. *Annu. Rev. Nutr.* **28**, 273-293.

**Matthews, R. P., Lorent, K., Manoral-Mobias, R., Huang, Y., Gong, W., Murray, I. V. J., Blair, I. A. and Pack, M.** (2009). TNFα-dependent hepatic steatosis and liver degeneration caused by mutation of zebrafish s-adenosylhomocysteine hydrolase. *Development* **136**, 865-875.

**McAllister, S. D. and Glass, M.** (2002). CB1 and CB2 receptor-mediated signalling: a focus on endocannabinoids. *Prostaglandins Leukot. Essent. Fatty Acids* **66**, 161-171.
**Migliarini, B. and Carnevali, O.** (2008). Anandamide modulates growth and lipid metabolism in the zebrafish Danio rerio. *Mol. Cell. Endocrinol.* **286**, S12-S16.
**Mukhopadhyay, B., Cinar, R., Yin, S., Liu, J., Tam, J., Godlewski, G., Harvey-White, J., Mordi, I., Cravatt, B. F., Lotersztajn, S. et al.** (2011). Hyperactivation of anandamide synthesis and regulation of cell-cycle progression via cannabinoid type 1 (CB1) receptors in the regenerating liver. *Proc. Natl. Acad. Sci. U.S.A.* **108**, 6323-6328.
**Munro, S., Thomas, K. L. and Abu-Shaar, M.** (1993). Molecular characterization of a peripheral receptor for cannabinoids. *Nature* **365**, 61-65.
**Nissim, S., Sherwood, R. I., Wucherpfennig, J., Saunders, D., Harris, J. M., Esain, V., Carroll, K. J., Frechette, G. M., Kim, A. J., Hwang, K. L. et al.** (2014). Prostaglandin E2 regulates liver versus pancreas cell-fate decisions and endodermal outgrowth. *Dev. Cell* **28**, 423-437.
**Ozanne, S. E.** (2014). Epigenetics and metabolism in 2014: metabolic programming —knowns, unknowns and possibilities. *Nat. Rev. Endocrinol.* **11**, 67-68.
**Pagotto, U., Marsicano, G., Cota, D., Lutz, B. and Pasquali, R.** (2006). The emerging role of the endocannabinoid system in endocrine regulation and energy balance. *Endocr. Rev.* **27**, 73-100.
**Pai, W.-Y., Hsu, C.-C., Lai, C.-Y., Chang, T.-Z., Tsai, Y.-L. and Her, G. M.** (2013). Cannabinoid receptor 1 promotes hepatic lipid accumulation and lipotoxicity through the induction of SREBP-1c expression in zebrafish. *Transgenic Res.* **22**, 823-838.
**Palazuelos, J., Ortega, Z., Diaz-Alonso, J., Guzman, M. and Galve-Roperh, I.** (2012). CB2 cannabinoid receptors promote neural progenitor cell proliferation via mTORC1 signaling. *J. Biol. Chem.* **287**, 1198-1209.
**Parsons, M. J., Pisharath, H., Yusuff, S., Moore, J. C., Siekmann, A. F., Lawson, N. and Leach, S. D.** (2009). Notch-responsive cells initiate the secondary transition in larval zebrafish pancreas. *Mech. Dev.* **126**, 898-912.
**Pascale, R. M., Marras, V., Simile, M. M., Daino, L., Pinna, G., Bennati, S., Carta, M., Seddaiu, M. A., Massarelli, G. and Feo, F.** (1992). Chemoprevention of rat liver carcinogenesis by S-adenosyl-L-methionine: a long-term study. *Cancer Res.* **52**, 4979-4986.
**Passeri, M. J., Cinaroglu, A., Gao, C. and Sadler, K. C.** (2009). Hepatic steatosis in response to acute alcohol exposure in zebrafish requires sterol regulatory element binding protein activation. *Hepatology* **49**, 443-452.
**Pisanti, S., Picardi, P., D'Alessandro, A., Laezza, C. and Bifulco, M.** (2013). The endocannabinoid signaling system in cancer. *Trends Pharmacol. Sci.* **34**, 273-282.
**Psychoyos, D., Vinod, K. Y., Cao, J., Xie, S., Hyson, R. L., Wlodarczyk, B., He, W., Cooper, T. B., Hungund, B. L. and Finnell, R. H.** (2012). Cannabinoid receptor 1 signaling in embryo neurodevelopment. *Birth Defects Res. B Dev. Reprod. Toxicol.* **95**, 137-150.
**Radford, E. J., Ito, M., Shi, H., Corish, J. A., Yamazawa, K., Isganaitis, E., Seisenberger, S., Hore, T. A., Reik, W., Erkek, S. et al.** (2014). In utero undernourishment perturbs the adult sperm methylome and intergenerational metabolism. *Science* **345**, 1255903-1255903.
**Sander, J. D., Cade, L., Khayter, C., Reyon, D., Peterson, R. T., Joung, J. K. and Yeh, J.-R. J.** (2011). Targeted gene disruption in somatic zebrafish cells using engineered TALENs. *Nat. Biotechnol.* **29**, 697-698.
**Shimano, H., Shimomura, I., Hammer, R. E., Herz, J., Goldstein, J. L., Brown, M. S. and Horton, J. D.** (1997). Elevated levels of SREBP-2 and cholesterol synthesis in livers of mice homozygous for a targeted disruption of the SREBP-1 gene. *J. Clin. Invest.* **100**, 2115-2124.
**Shyh-Chang, N., Daley, G. Q. and Cantley, L. C.** (2013). Stem cell metabolism in tissue development and aging. *Development* **140**, 2535-2547.
**Sinclair, K. D. and Watkins, A. J.** (2014). Parental diet, pregnancy outcomes and offspring health: metabolic determinants in developing oocytes and embryos. *Reprod. Fertil. Dev.* **26**, 99.
**Sinclair, K. D., Allegrucci, C., Singh, R., Gardner, D. S., Sebastian, S., Bispham, J., Thurston, A., Huntley, J. F., Rees, W. D., Maloney, C. A. et al.** (2007). DNA methylation, insulin resistance, and blood pressure in offspring determined by maternal periconceptional B vitamin and methionine status. *Proc. Natl. Acad. Sci. USA* **104**, 19351-19356.
**Sipe, J. C., Waalen, J., Gerber, A. and Beutler, E.** (2005). Overweight and obesity associated with a missense polymorphism in fatty acid amide hydrolase (FAAH). *Int. J. Obes.* **29**, 755-759.
**Sugiura, T., Kondo, S., Sukagawa, A., Nakane, S., Shinoda, A., Itoh, K., Yamashita, A. and Waku, K.** (1995). 2-Arachidonoylglycerol: a possible endogenous cannabinoid receptor ligand in brain. *Biochem. Biophys. Res. Commun.* **215**, 89-97.
**Sun, X., Xie, H., Yang, J., Wang, H., Bradshaw, H. B. and Dey, S. K.** (2010). Endocannabinoid signaling directs differentiation of trophoblast cell lineages and placentation. *Proc. Natl. Acad. Sci. USA* **107**, 16887-16892.
**Swanson, D. A., Liu, M.-L., Baker, P. J., Garrett, L., Stitzel, M., Wu, J., Harris, M., Banerjee, R., Shane, B. and Brody, L. C.** (2001). Targeted disruption of the methionine synthase gene in mice. *Mol. Cell. Biol.* **21**, 1058-1065.
**Teixeira-Clerc, F., Belot, M.-P., Manin, S., Deveaux, V., Cadoudal, T., Chobert, M.-N., Louvet, A., Zimmer, A., Tordjmann, T., Mallat, A. et al.** (2010). Beneficial paracrine effects of cannabinoid receptor 2 on liver injury and regeneration. *Hepatology* **52**, 1046-1059.
**Thisse, C. and Thisse, B.** (2008). High-resolution in situ hybridization to whole-mount zebrafish embryos. *Nature Prot.* **3**, 59-69.
**Tomasi, M. L., Ramani, K., Lopitz-Otsoa, F., Rodríguez, M. S., Li, T. W. H., Ko, K., Yang, H., Bardag-Gorce, F., Iglesias-Ara, A., Feo, F. et al.** (2010). S-adenosylmethionine regulates dual-specificity mitogen-activated protein kinase phosphatase expression in mouse and human hepatocytes. *Hepatology* **51**, 2152-2161.
**Walker, A. K., Jacobs, R. L., Watts, J. L., Rottiers, V., Jiang, K., Finnegan, D. M., Shioda, T., Hansen, M., Yang, F., Niebergall, L. J. et al.** (2011). A conserved SREBP-1/phosphatidylcholine feedback circuit regulates lipogenesis in metazoans. *Cell* **147**, 840-852.
**Watson, S., Chambers, D., Hobbs, C., Doherty, P. and Graham, A.** (2008). The endocannabinoid receptor, CB1, is required for normal axonal growth and fasciculation. *Mol. Cell. Neurosci.* **38**, 89-97.
**Yin, C., Evason, K. J., Maher, J. J. and Stainier, D. Y. R.** (2012). The basic helix-loop-helix transcription factor, heart and neural crest derivatives expressed transcript 2, marks hepatic stellate cells in zebrafish: Analysis of stellate cell entry into the developing liver. *Hepatology* **56**, 1958-1970.
**Yuan, M., Breitkopf, S. B., Yang, X. and Asara, J. M.** (2012). A positive/negative ion–switching, targeted mass spectrometry–based metabolomics platform for bodily fluids, cells, and fresh and fixed tissue. *Nat. Protoc.* **7**, 872-881.

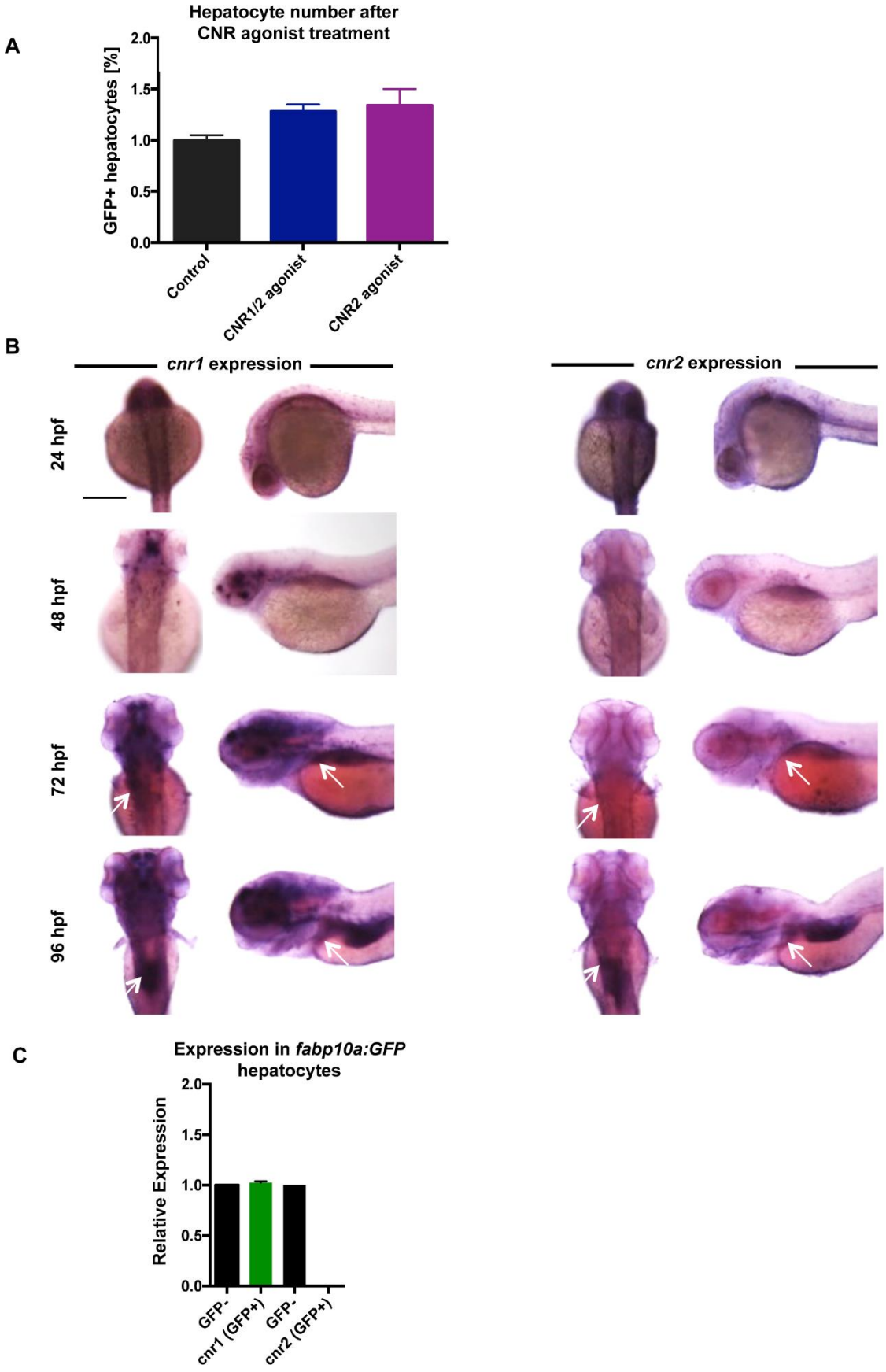


Development • Supplementary information

**Figure S1. Cannabinoid receptor expression in the developing zebrafish**

A) FACS quantification of GFP-positive hepatocytes in *fabp10a:GFP* embryos treated with cannabinoid agonists from 24-72hpf. % of GFP positive cells were normalized to controls. Mean±s.e.m., n=5 groups of 10 pooled embryos; p=0.08, one-way ANOVA analysis.

B) Dorsal and lateral *in situ* hybridization images at 24, 48, and 72hpf showing that *cnr1* and *cnr2* are expressed in the developing central nervous system, endoderm (arrow), and liver regions (arrow). Scale bar = 0.2 mm.

C) qRT-PCR detects *cnr1* expression in pooled FACS-sorted GFP-positive cells (~200,000 cells) from wild type *fabp10a:GFP* normalized to expression in the GFP-negative cell fraction, which includes the central nervous system. *cnr2* is detectable in the non-hepatocyte (GFP-negative) fraction, but not in the hepatocytes.

Development • Supplementary information

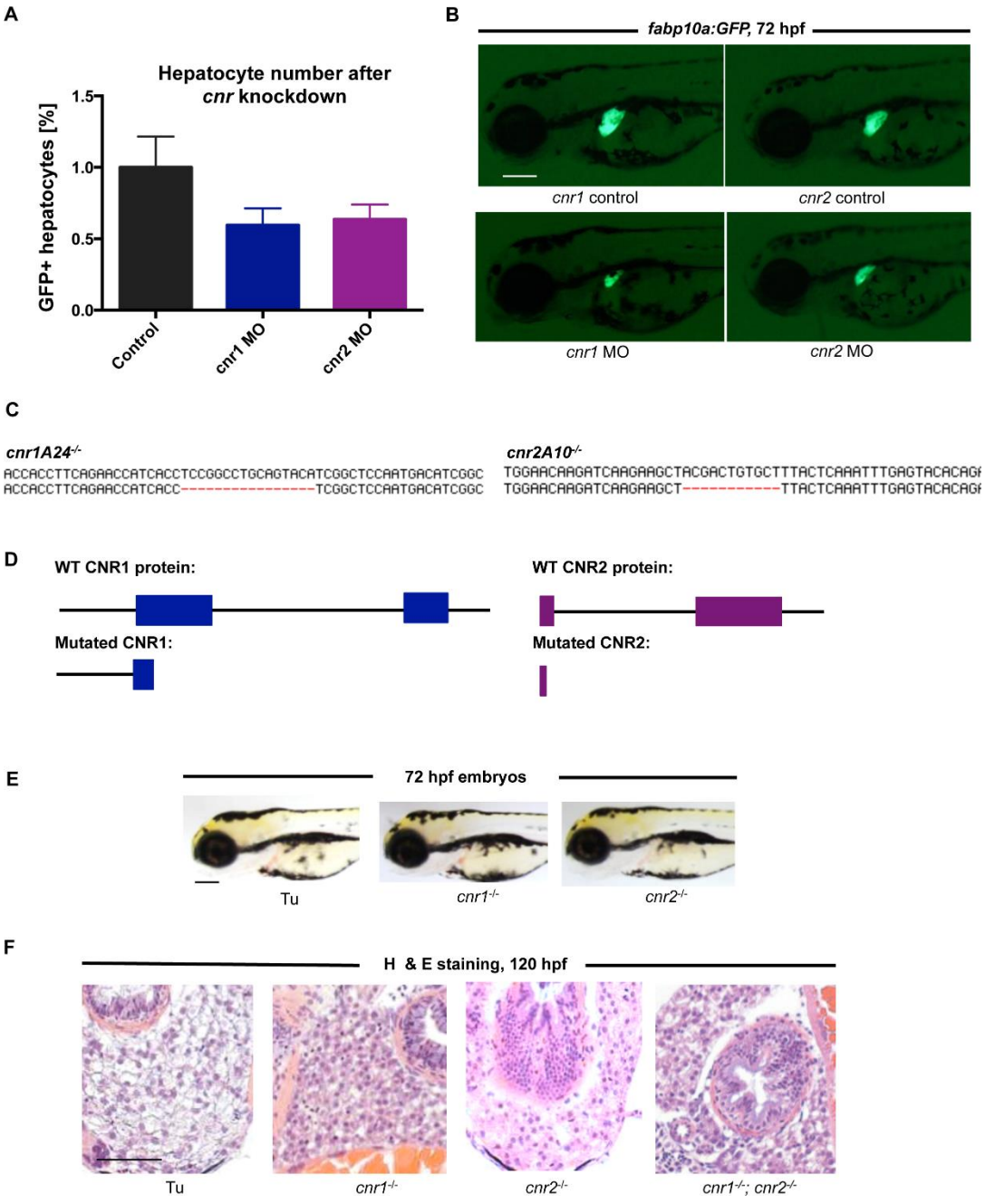


**Figure S2. Characterization of cannabinoid receptor mutants and morphants**

A) FACS quantification of *fabp10a:GFP* embryos injected with *cnr1* and *cnr2* morpholinos. Morphant embryos at 72hpf show a decreased number of GFP-positive hepatocytes. Mean±s.e.m., n=5 groups of 10 pooled embryos; p=0.18, one-way ANOVA analysis.

Development • Supplementary information

B) Fluorescent micrographs showing that morpholino knockdown of *cnr1* or *cnr2* in *fabp10a:GFP* reporter fish leads to smaller livers at 72hpf. Scale bar = 0.2 mm.

C) Depiction of wild type and mutant sequence of the TALEN target region in the *cnr1* and *cnr2* genes.

D) Small deletions in the DNA sequence lead to an early stop codon in the first exon of both *cnr1* and *cnr2*.

E) Brightfield images of *cnr1*$^{-/-}$ and *cnr2*$^{-/-}$ zebrafish at 72hpf reveal no gross anatomical abnormalities or significant developmental delay compared to wild type animals. Scale bar = 0.2 mm.

F) H & E staining of transverse sections in 120hpf larvae reveals similarly abnormal liver histology in *cnr1*$^{-/-}$*; cnr2*$^{-/-}$ double mutants compared to histology found in the *cnr1*$^{-/-}$ and *cnr2*$^{-/-}$ single mutants shown in **Figure 3A**. Scale bar = 0.1 mm.

Development • Supplementary information

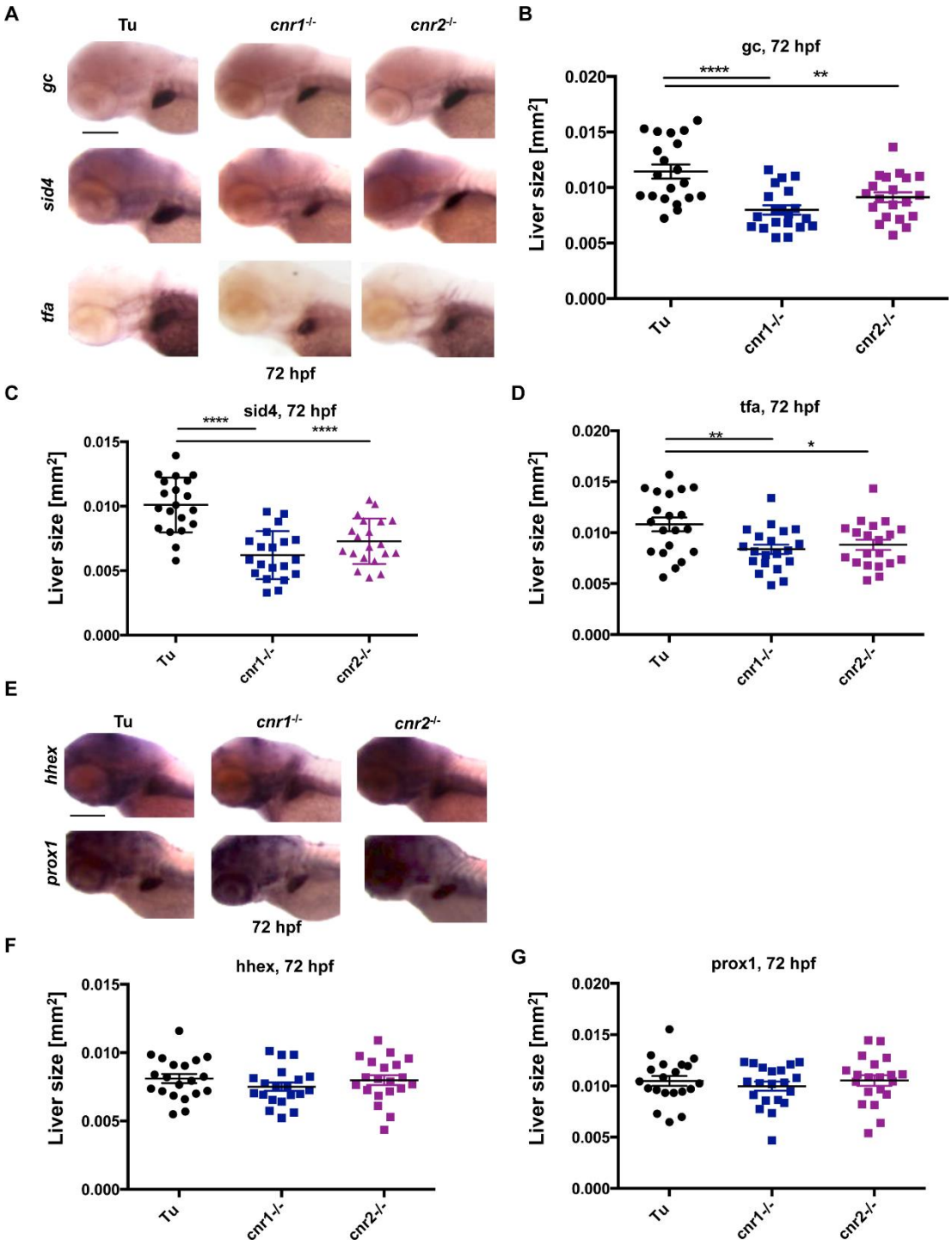


**Figure S3. Examination of additional hepatic markers in *cnr1*$^{-/-}$ and *cnr2*$^{-/-}$ mutants**

A) Representative *in situ* hybridization images and scatter plots quantifying (B-D) expression of

Development • Supplementary information

additional hepatocyte markers in *cnr1*$^{-/-}$ and *cnr2*$^{-/-}$ mutants at 72hpf. Expression of *group-specific component (vitamin D binding protein*, *gc)*, *secreted immunoglobulin domain 4* (*sid4),* and *transferrin (tfa)* were all reduced in *cnr1*$^{-/-}$ and *cnr2*$^{-/-}$ mutants. These results confirm smaller liver size and exclude a dependence on *fabp10a* expression when cannabinoid receptors are knocked out in these mutants. Data are represented as mean±s.e.m. with one-way ANOVA analysis. Results shown represent one independent experiment of triplicate experiments which yielded similar results, n >15 for each experiment, *p<0.05, **p<0.01, ***p<0.001, ****p<0.0001. Scale bar = 0.2 mm.

E) Representative *in situ* hybridization images and scatter plots quantifying (F-G) expression of hepatic progenitor markers *hhex* and *prox1* at 72hpf. Hepatic progenitors remain unchanged in *cnr1*$^{-/-}$ and *cnr2*$^{-/-}$ mutants at 72hpf. These data indicate that disruption of signaling through cannabinoid receptors impacts hepatic differentiation. Data are represented as mean±s.e.m. with one-way ANOVA analysis. Results shown represent one independent experiment of triplicate experiments which yielded similar results, n >15 for each experiment, p=0.42 and p=0.68 for *hhex* and *prox1,* respectively. Scale bar = 0.2 mm.

Development • Supplementary information

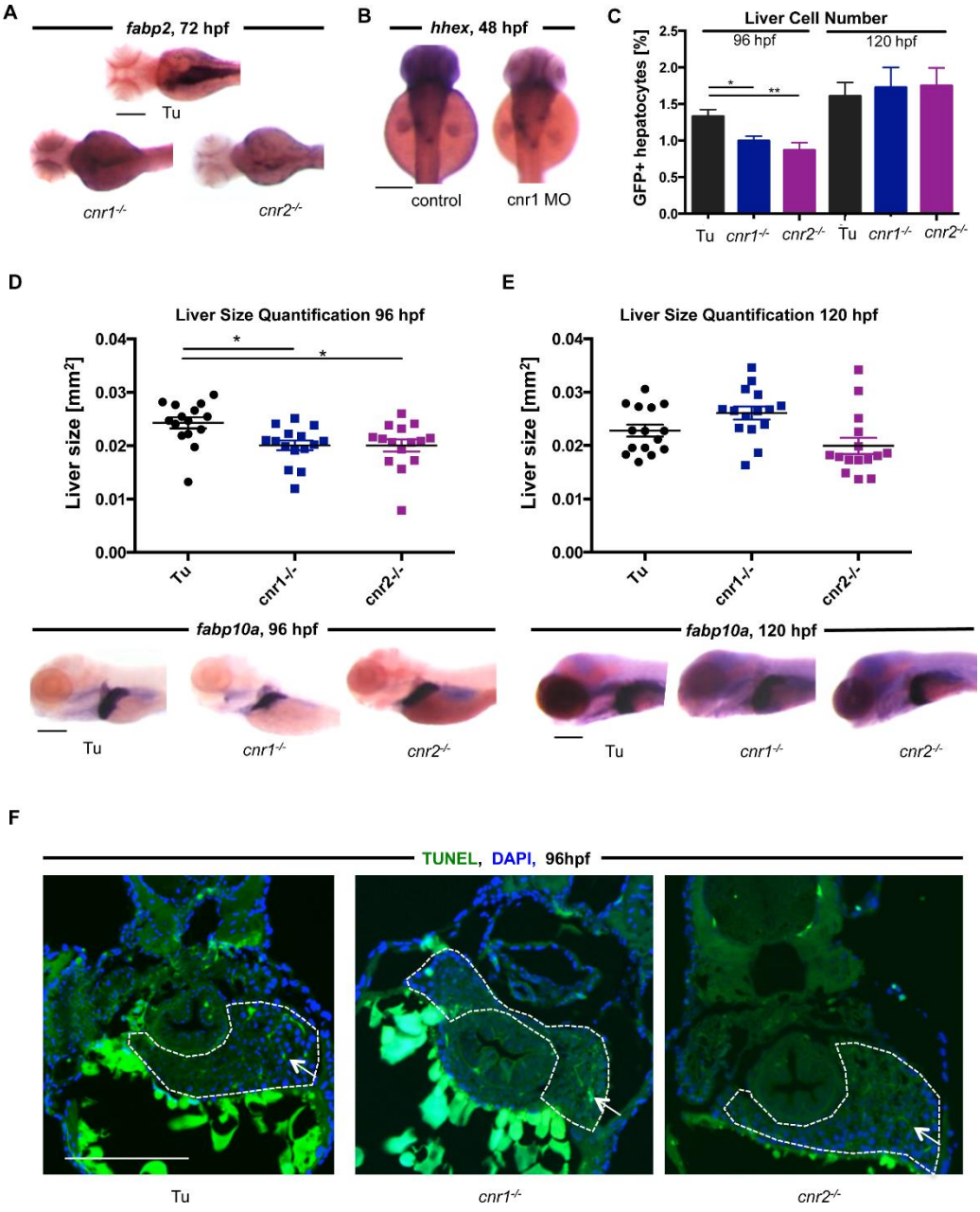


**Figure S4. Mechanisms of liver size changes in cannabinoid receptor mutants**

A) *in situ* hybridization shows reduction in the intestinal reporter *fabp2* in *cnr1*$^{-/-}$ (62.5% with phenotype, n=40) and *cnr2*$^{-/-}$ mutants at 72hpf (57.1% with phenotype, n-56). Scale bar = 0.2 mm.

Development • Supplementary information

B) *in situ* hybridization images depict the size distribution of *hhex* expression after morpholino knockdown of *cnr1* and *cnr2*. Morphant embryos do not exhibit differences in *hhex* liver progenitor expression. Scale bar = 0.2 mm.

C) FACS quantification of *fabp10a:GFP* WT embryos compared to *cnr1*$^{-/-}$ and *cnr2*$^{-/-}$ mutants at 96 and 120hpf. % of GFP+ cells were normalized to controls. Mean±s.e.m. n= 7-10 pooled samples of 10 embryos each, one-way ANOVA analysis, *p<0.05 *fabp10a:GFP* vs. *cnr1*$^{-/-}$ and **p<0.01 *fabp10a:GFP* vs *cnr2*$^{-/-}$.

D - E) Scatter plot and representative *in situ* hybridization images showing liver size of *cnr1*$^{-/-}$ and *cnr2*$^{-/-}$ mutants at 96hpf (C) and 120hpf (D) based on liver morphometric measurements using ImageJ. At 96hpf, livers in mutants are still significantly smaller than controls, but this difference disappears by 120hpf. Data are represented as mean±s.e.m. with one-way ANOVA analysis, *p<0.05 for Tu compared to *cnr1*$^{-/-}$ and *cnr2*$^{-/-}$ at 96hpf only. Scale bar = 0.2 mm.

F) TUNEL staining in 96hpf embryos reveals no difference in cell death in the developing livers (outlined) of wild type (4.6% TUNEL positive cells, marked by white arrows) compared to *cnr1*$^{-/-}$ (3.9%) and *cnr2*$^{-/-}$ mutants (3.0%), indicating that cell death does not substantially contribute to small liver size in cannabinoid receptor mutants. Percentages represent average of n=3, Scale bar = 0.2 mm.

Development • Supplementary information

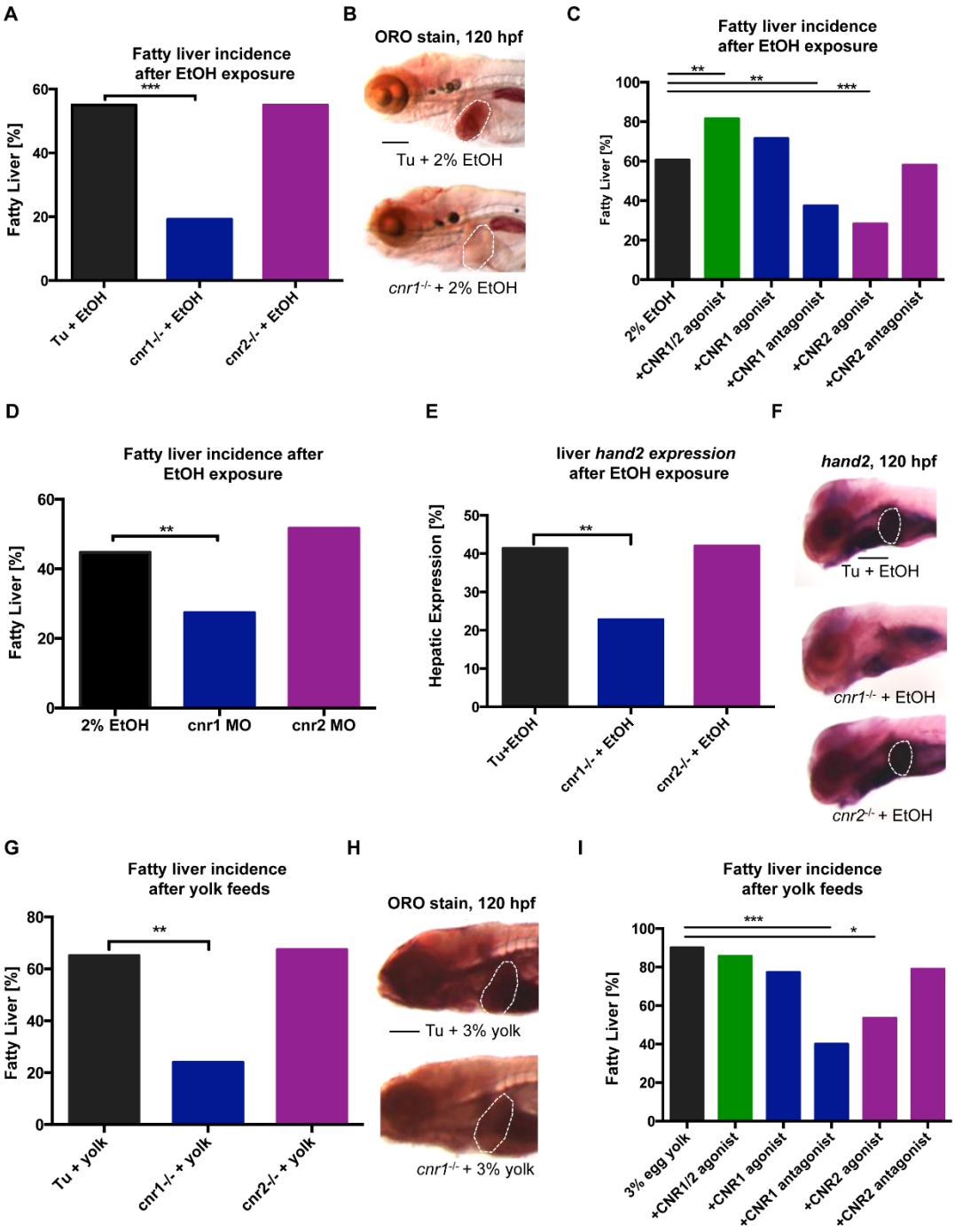


**Figure S5. *cnr1* mutants and morphants and treatment with CNR1 antagonist protects from hepatic steatosis and *hand2* induction**

A) After inducing liver injury with ethanol (2% treatment from 96-120hpf), *cnr1*$^{-/-}$, but not *cnr2*$^{-/-}$,

Development • Supplementary information

mutants at 120hpf are protected from acquiring fatty liver (outlined) as assessed by Oil Red O (ORO) staining (B). Fisher's Exact test, n>30, ***p<0.001 compared to control treatment. Scale bar = 0.2 mm.

C) Co-treatment with cannabinoid agonists and antagonists from 96-120hpf reveal that CNR1/2 and CNR1 agonists increase steatosis incidence after ethanol exposure while the CNR1 antagonist and CNR2 agonists prevent steatosis induction. Fisher's Exact test, n >30, **p<0.01 and ***p<0.001.

D) *cnr1* but not *cnr2* morphants are protected from induction of steatosis after ethanol exposure. Fisher's Exact test, n >30, **p<0.01.

E) *cnr1*$^{-/-}$ mutants have decreased hepatic stellate cell activation after ethanol exposure based on hepatic *hand2* expression (outlined) by *in situ* hybridization (F). Fisher's Exact test, n >30, **p<0.01. Scale bar = 0.2 mm.

G) *cnr1*$^{-/-}$ but not *cnr2*$^{-/-}$ mutants fed a high-fat egg yolk diet from 96-120hpf are protected from fatty liver (outlined), as indicated by Oil Red O staining (H). Fisher's Exact test, n >30, **p<0.01 vs. controls. Scale bar = 0.2 mm.

I) Co-treatment with cannabinoid agonists and antagonists reveals that CNR1 antagonist and CNR2 agonist prevents steatosis induction in a high-fat diet egg yolk feeding model. Fisher's Exact Test, n >30, *p<0.05 and ***p<0.001 vs. controls.

Development • Supplementary information

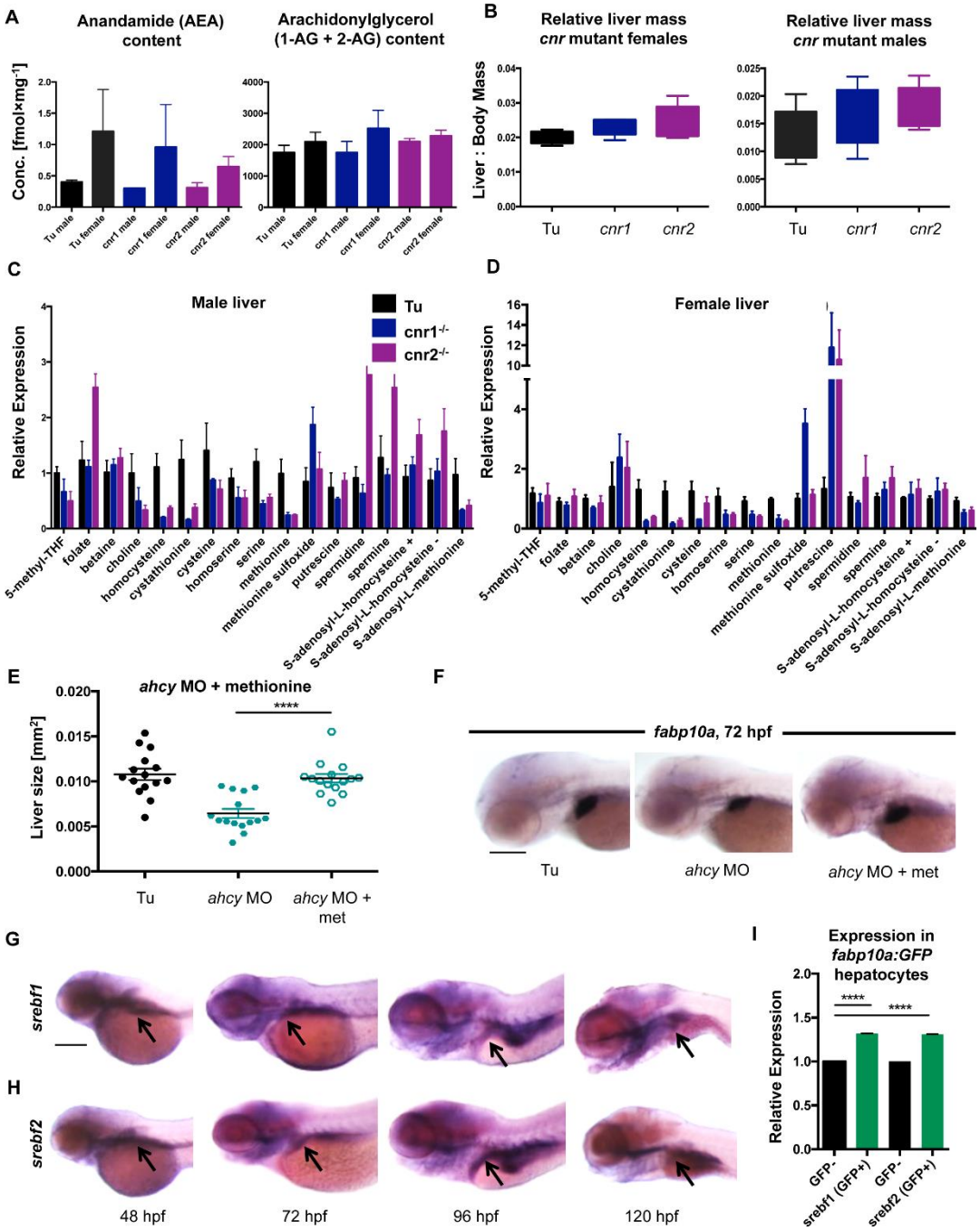


**Figure S6. Altered methionine metabolism compounds in cannabinoid receptor mutants**

A) Anandamide (AEA) and Arachidonylglycerol (1-AG and 2-AG) content in adult liver samples were measured by liquid chromatography/tandem mass spectrometry, revealing no statistically significant differences between control and mutant samples. Data are represented as mean±s.e.m., n=2.

Development • Supplementary information

B) Liver-to-body mass ratio measurements in female and male adult *cnr1*$^{-/-}$ and *cnr2*$^{-/-}$ mutants show no difference in liver size between cannabinoid receptor mutants and controls by adulthood. Mean±s.e.m., n=5 fish for each condition.

C) Polar metabolomics analysis reveals relative levels of methionine pathway metabolites from male and D) female *cnr1*$^{-/-}$ or *cnr2*$^{-/-}$ adult livers. Data are represented as mean±s.e.m., n=3.

E) Scatter plot and F) representative *in situ* hybridization images showing that morpholino knockdown of *ahcy* results in smaller liver size at 72hpf, while treatment with methionine (100μM) from 24-72hpf can rescue this liver size defect. Data are represented as mean±s.e.m. with one-way ANOVA analysis. Results shown represent one independent experiment of triplicate experiments which yielded similar results, n>15, ****p<0.0001 for *ahcy* morphant compared to methionine rescue treatment group. Scale bar = 0.2 mm.

G-H) *In situ* hybridization images at 48, 72, 96, and 120hpf showing that *srebf1* (G) and *srebf2* (H) are expressed in endodermal organs, particularly the developing pharynx and gut (arrow). Scale bar = 0.2 mm.

I) qRT-PCR detects *srebf1* and *srebf2* expression in pooled FACS-sorted GFP-positive cells (~200,000 cells) from wild-type *fabp10a:GFP* normalized to expression in the GFP-negative cell fraction. Both genes are highly enriched in the hepatocytes. Mean±s.e.m., Student's t-test, ****p<0.0001 for GFP-negative vs GFP-positive when detecting both *srebf1* and *srebf2*.

Development • Supplementary information

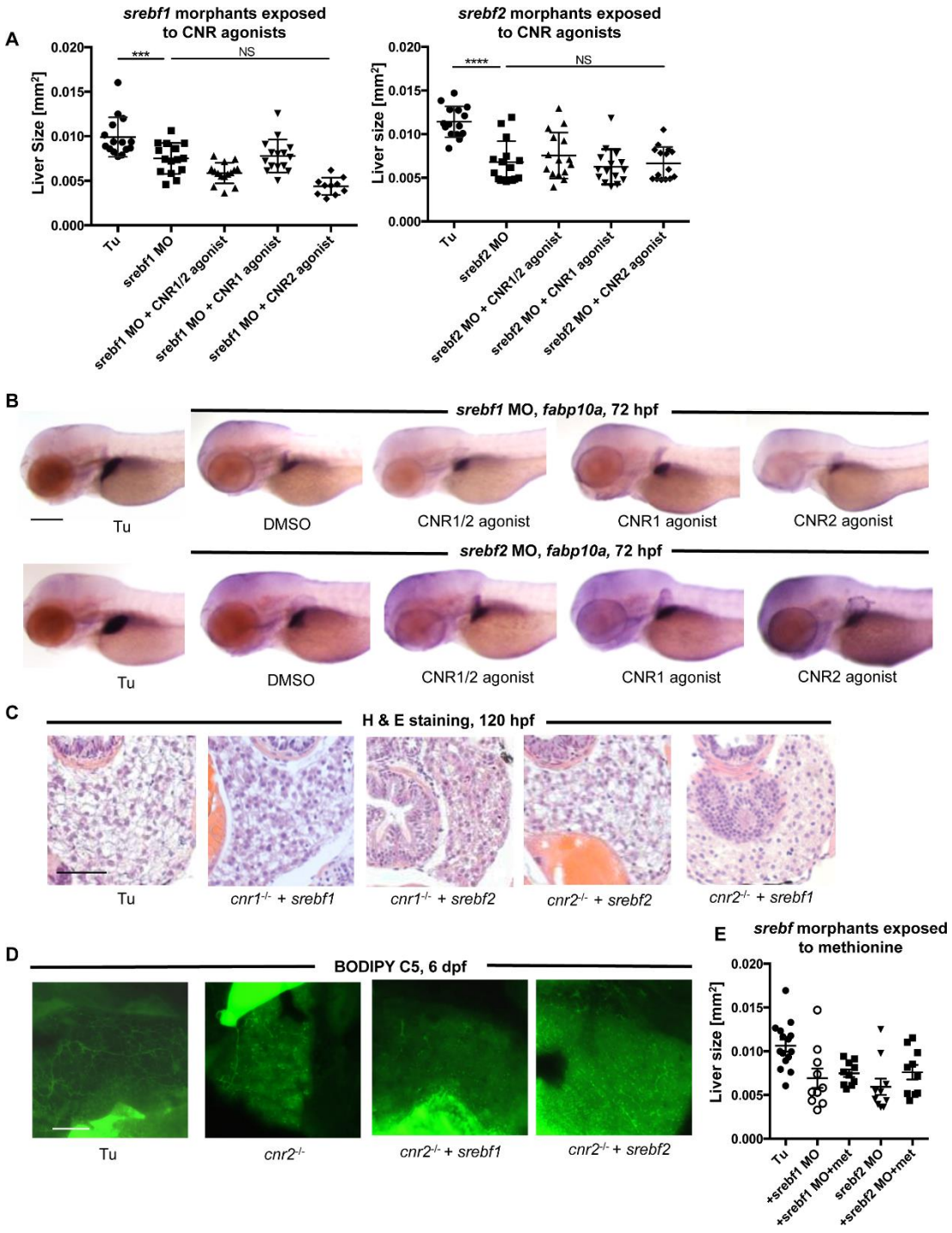


**Figure S7. Role of *srebf1* and *srebf2* in liver development**

A-B) Scatter plot based on liver morphometric measurements and B) representative *in situ* hybridization images at 72hpf showing reduced liver size of *srebf1* and *srebf2* morphants. CNR1/2 agonist O2545, CNR1 agonist L-HCl, and CNR2 agonist JWH015 treatment from 24-72hpf fail to rescue liver growth in *srebf1* and *srebf2* morphants. Data are represented as mean±s.e.m. with one-way ANOVA analysis, n>15, ***p<0.001 control vs. *srebf1* morphant, ****p<0.0001 for control vs *srebf2* morphant. Scale bar = 0.2 mm.

Development • Supplementary information

C) H&E staining of transverse sections in 120hpf larvae shows that overexpression of *srebf1* but not *srebf2* can partially restore wild type liver histology when compared to wild type, *cnr1*$^{-/-}$, and *cnr2*$^{-/-}$ sections in **Figure 6C**. When *srebf1* is overexpressed in the *cnr1*$^{-/-}$ background, n=6/9 had normal liver cellular architecture while n=7/8 *cnr2*$^{-/-}$ larvae were similarly rescued after *srebf1* mRNA overexpression. Scale bar = 0.1 mm.

D) Confocal microscopy images of livers in *cnr2*$^{-/-}$ mutant larvae with and without *srebf1* and *srebf2* overexpression after BODIPY C5 incorporation. There were no major differences between *cnr2*$^{-/-}$ mutants and larvae with mRNA overexpression in biliary tree organization or lipid deposition. Scale bar = 20 μm.

E) catter plot based on liver morphometric measurements of *srebf1* and *srebf2* morphants treated with methionine. Exposure to methionine from 24-72hpf did not alter the diminished liver size of morphants. Mean±s.e.m.

Development • Supplementary information

## Supplemental Materials and Methods

### *TUNEL Staining*

TUNEL staining was performed on paraffin-embedded transverse sections from embryo samples using the FragEL DNA Fragmentation Detection Kit (Millipore) with manufacturer's protocol for paraffin-embedded sections. Slides were mounted using DAPI mounting medium.

### *Endocannabinoid measurements*

The tissue levels of endocannabinoids were measured by stable isotope dilution liquid chromatography/tandem mass spectrometry (LC-MS/MS) as described previously (Mukhopadhyay et al., 2011).

### *Generation of* srebf1 *and* srebf2 *mRNA probes*

*srebf1* and *srebf2* were amplified from wild type zebrafish cDNA using the following primers: *srebf1* (5'ATGAATCTGTCTTTTGACGACACTTCT 3', 5'TTAGGTGGAGGTGACGGTG 3') and *srebf2* (5'ATGGACGCCTCGGAGTTTAT 3', 5' TTATGACGCAGCGATGGTGG 3'). The PCR products were cloned into the TOPO-TA Cloning vector (Life Technologies) for mRNA probe synthesis.

Development • Supplementary information

**Table S1: qRT-PCR primers**

| Gene | Forward Primer | Reverse Primer |
|---|---|---|
| ***fabp10a*** | GATGGAGGAAAGCTGGTCTG | TCCTGATCATGGTGGTTCCT |
| ***ahcy*** | ACCAGACAGCACAACGTCAA | AGACCCGGCATCTCATTCT |
| ***mthfr*** | GTCTGGAGCGGTCAATCTTATC | CGGGATGCCAAGTGATGT |
| ***bhmt*** | GCATGGAGTTACACCTGGAGA | CACAGTCTTCACACAGGTCAGG |
| ***srm*** | CGAAGTTCCAGGATGTGATG | GGTGGCAGCAGAGAGGTAGA |
| ***srebf1*** | GTCTGTCGGCTTCACCAATC | GAGAGTCGGCCTTAATGAACTG |
| ***srebf2*** | ACCATACAGACGCTCTCCACA | GGTTTGGTGGTCAGAAGCAG |
| ***cnr1*** | ATCTGTTCTGGCGGATGG | GGTTGACGGTGGAGTTGAG |
| ***cnr2*** | GCAGAGCGTGAAAGGACAG | GATCGCCAGGATTAGAAGGA |

Development • Supplementary information

**Table S2: Morpholinos**

| Gene | Type | Conc. [µM] | Amount [ng] | Sequence |
|---|---|---|---|---|
| ***cnr1*** | ATG | 100 | ~4.15 | CTTTGAGGCCGGGAACAGCATGGTC |
| ***cnr1*** | splice | 100 | ~4.15 | GTGCTATCAACAACATACCTTTGTG |
| ***cnr2*** | ATG | 100 | ~4.15 | GTTCCAGTTTGTTCTCCATTTTCCC |
| ***cnr2*** | splice | 100 | ~4.15 | GCCATGAAACAAACAGTACCTGTGG |
| ***srebf1*** | ATG | 100 | ~4.15 | AAGTGTCGTCAAAAGACAGATTCAT |
| ***srebf1*** | splice | 100 | ~4.15 | AATCACTAAATAAGCTGACCTGTGC |
| ***srebf2*** | ATG | 100 | ~4.15 | GCGTCCATGTTTCTCCACCTTCTCT |
| ***srebf2*** | splice | 100 | ~4.15 | TGTGGTCAGACTCACCTGTGTGATT |
| ***ahcy*** | splice | 100 | ~4.15 | CTCAAAGTGTCTTTAAAACACACAC |
| *standard control* | | 100 | ~4.15 | CCTCTTACCTCAGTTACAATTTATA |

Development • Supplementary information

**Table S3: Chemicals**

| Chemical | Concentration |
|---|---|
| O2545 | 1 μM |
| leelamine hydrochloride | 10 μM |
| JWH015 | 1 μM |
| AM630 | 1 μM |
| Rimonabant | 1 μM |
| methionine | 100 μM |
| cysteine | 100 μM |

**Table S4: Antibodies**

| Antibody | Concentration | Catalog number |
|---|---|---|
| Anti-2F11 | 1:1000 | Abcam ab71286 |
| Anti-Methylated-lysine | 1:1000 | Abcam ab23366 |
| Peroxidase-Affinipure Goat Anti-Rabbit IgG | 1:1000 | Jackson Immunoresearch 111-035-144 |
| Goat anti-mouse IgG-FITC | 1:500 | Santa Cruz sc-2010 |

Development • Supplementary information